Chapter 2

Intra- and intermolecular C−H bond activation by bis(phenolate)pyridineiridium(III) complexes

2.1 Abstract

A bis(phenolate)pyridine pincer ligand (henceforth abbreviated as ONO) has been employed to support a variety of iridium complexes in oxidation states I, III, and IV. Complexes (ONO)IrL_2Me (L = PPh_3, PEt_3) react with I_2 to cleave the Ir−C bond and liberate MeI, apparently *via* a mechanism beginning with electron transfer to generate an intermediate Ir^{IV} complex, which can be isolated and characterized for the case L = PEt_3. The PPh_3 complex is transformed in benzene at 65°C to the corresponding phenyl complex, with loss of methane, and subsequently to a species resulting from metalation of a PPh_3 ligand. Labeling and kinetics studies indicate that PPh_3 is the initial site of C−H activation, even though the first observed product is that resulting from intermolecular benzene activation. C−H activation of acetonitrile has also been observed.

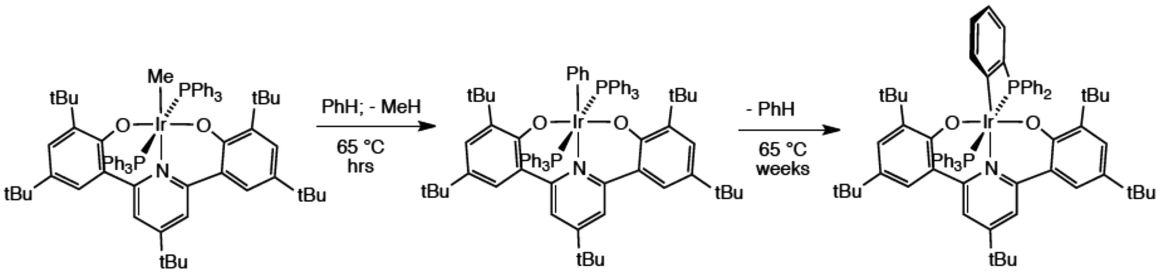

2.2 Introduction

Functionalization of alkanes, such as the selective oxidation of methane to methanol, has long been a desired goal of both academic and industrial research [1]. Much of the focus has been on routes involving C−H activation at a transition metal center followed by oxidative cleavage of the resulting C−M bond, which offer greater possibilities for good selectivity by avoiding radical-based pathways. (Yields of methanol from the direct reaction of methane with dioxygen, where radical pathways predominate, appear to be limited to about 5%, because methanol is more rapidly oxidized than methane, a consequence of its weaker C-H bond [1]d.) Platinum complexes have received a great deal of attention [2], starting with Shilov's seminal work on the $PtCl_4^{2-}/PtCl_6^{2-}$ system, which can oxidize methane to methanol with some selectivity [3], and including the platinum bipyrimidine system, which has achieved the most impressive performance to date, converting methane to methyl bisulfate in up to 70% yield [4].

However, none of this platinum-based chemistry has yet been shown to lead to a practical process, owing in part to low reactivity, and a good deal of research activity has turned to other metals. Iridium in particular has been a popular choice; many (primarily low-valent) Ir complexes have been reported to show good activity for C−H activation [5], and examples of oxidative functionalization with Ir systems are known as well [6]. Interconversions between Ir^{III} and Ir^{V} might be important in this chemistry, by analogy to the Shilov system, which involves Pt^{II} and Pt^{IV}. A separate program in our group has examined dianionic tricoordinate ("LX_2") pincer ligands for reactions involving high-valent early transition metal centers [7], and it occurred to us that such strongly electron donating, hard, and robust ligands might also be useful here, to provide more facile access to the relatively high Ir^{V} oxidation state.

We previously reported some chemistry of a bis(phenolate)-*N*-heterocyclic carbene ligand (OCO) that supports complexes in the oxidation states Ir^{I}, Ir^{III}, and Ir^{IV}, but no C−H activation chemistry was demonstrated [8]. Here we report on two related bis(phenolate)pyridine ligands (ONO = pyridine-2,6-bis[2-(4,6-di-*tert*-butylphenolate)]; ONO^{tBu} = 4-*tert*-butylpyridine-2,6-bis[2-(4,6-di-*tert*-butylphenolate)] 2.1), which also enable synthesis of a wide variety of Ir^{I}, Ir^{III}, and Ir^{IV} complexes. In addition, the Ir^{III} complex $(ONO^{tBu})Ir(PPh_3)_2Me$ readily activates C−H bonds of benzene and acetonitrile, as well as of coordinated triphenylphosphine.

2.3 Results and Discussion

2.3.1 Synthesis and Characterization of Ir^{I} complexes

Because Ir^{III} is usually highly substitutionally inert, we decided to enter the Ir(ONO) system *via* Ir^{I}. H_2(ONO) [9] was doubly deprotonated with NaH, followed by metalation with $[Ir(cod)Cl]_2$, giving

Figure 2.1. The ONO and ONO$^{t\mathrm{Bu}}$ ligands.

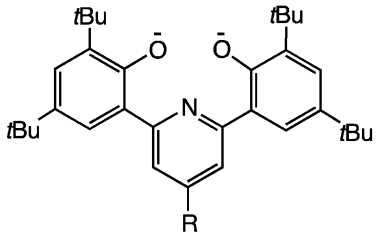

Na[Ir(cod)(ONO)], **1**, which was characterized by NMR and mass spectrometry. The symmetry of the ^{1}H NMR (only two *tert*-butyl peaks, for example) is consistent with either a five-coordinate structure or a fluxional four-coordinate structure, with the phenolates coordinated to Na^+ and Ir rapidly interchanging (**1a** and **1b**, respectively, in Scheme 2.1). The latter appears more likely on two grounds: First, the related OCO complex of Ir^I was crystallized (as the $[K(18\text{-crown-6})]^+$ salt **2**) and shown to have a structure analogous to that of **1b** [8]. Second, attempted crystallization of **1** in the presence of 15-crown-5 (attempts to crystallize **1** without 15-crown-5 were unsuccessful) instead yielded **3**, the result of C−H activation at the 3-position of the central pyridine ring (Figure 2.2).

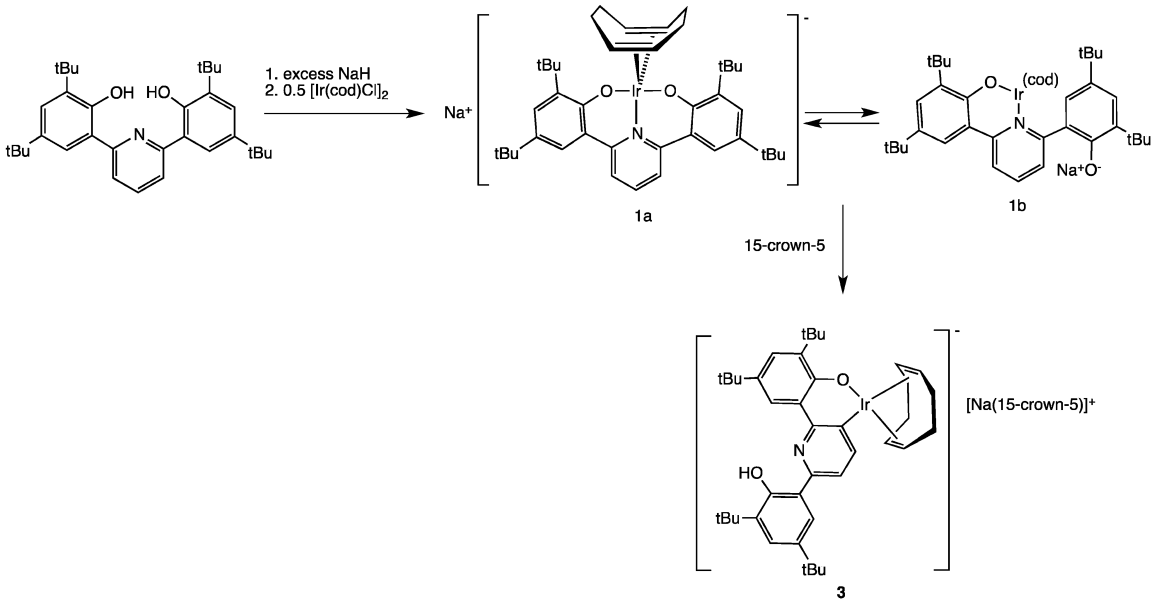

Scheme 2.1. Synthesis of Na[Ir(cod)(ONO)], **1**.

C−H activation probably results from complexation of the sodium ion by 15-crown-5, making it too sterically bulky to coordinate to the pendant phenolate in structure **1b**, and thus labilizing the pyridine, which can flip over to allow the oxidative addition of the 3-C−H bond; the resulting

Figure 2.2. Crystal structure of **3**. The nearest Na(15-crown-5) is located above the plane of the ligand and has been omitted for clarity. Because of crystal sensitivity, the structure obtained was only of sufficient quality to establish connectivity.

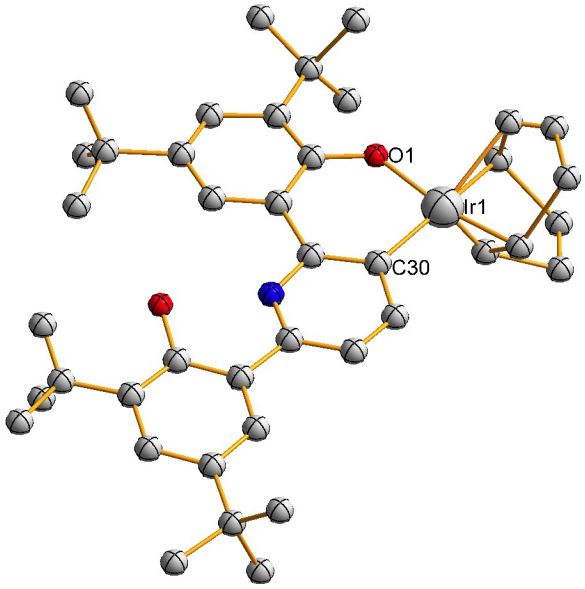

iridium (III) hydride is deprotonated by the pendant phenolate to regenerate square-planar Ir^{I}. This reactivity appears to require a solution of **1** to contain the isomer **1b**, either as the sole species present or, at least, in equilibrium with **1a**. C−H activation in preference to *N*-coordination of a pyridine ring has been observed previously for an NHC-pyridine ligand [10]; in that case (and probably here as well) *N*-coordination is disfavored sterically.

In order to prevent this unwanted ligand C−H activation, we prepared $H_2(ONO^{tBu})$, with an additional *tert*-butyl group to inhibit C−H activation of the pyridine linker. The synthesis of the ligand, which was straightforward and analogous to that of $H_2(ONO)$, is shown in Scheme 2.2. Deprotonation of $H_2(ONO^{tBu})$ with NaH, followed by metalation with half an equivalent (i.e. one Ir per ligand) of $[Ir(cod)Cl]_2$, gave deep red $[NaIr(cod)(ONO^{tBu})]_2$ (**4**, Scheme 2.3), shown crystallographically to have a dimeric structure (Figure 2.3). Unlike ONO complex **1**, **4** is readily soluble in pentane, presumably because the hydrophilic Na_2O_2 core is surrounded by a lipophilic shell of *tert*-butyl-substituted phenyl rings. As with **1**, the ^1H NMR spectrum indicates either a more symmetric structure in solution or a fluxional process; on cooling to −100°C, the spectrum exhibited some line broadening, but no decoalescence of peaks. **4** reacts with CO to give $Ir_4(CO)_{12}$ and is reduced by H_2 to metallic Ir.

If instead a full equivalent of $[Ir(cod)Cl]_2$ is added to one equivalent of $Na_2(ONO^{tBu})$, the orange diiridium complex $[Ir(cod)]_2(ONO^{tBu})$ (**5**) is obtained. **5** may also be prepared from **4** plus half an equivalent of $[Ir(cod)Cl]_2$, but **4** is not formed from **5** and additional $Na_2(ONO^{tBu})$ (Scheme 2.3). The two iridium atoms in **5** are inequivalent: Ir1 is five-coordinate, bound to both oxygens and the

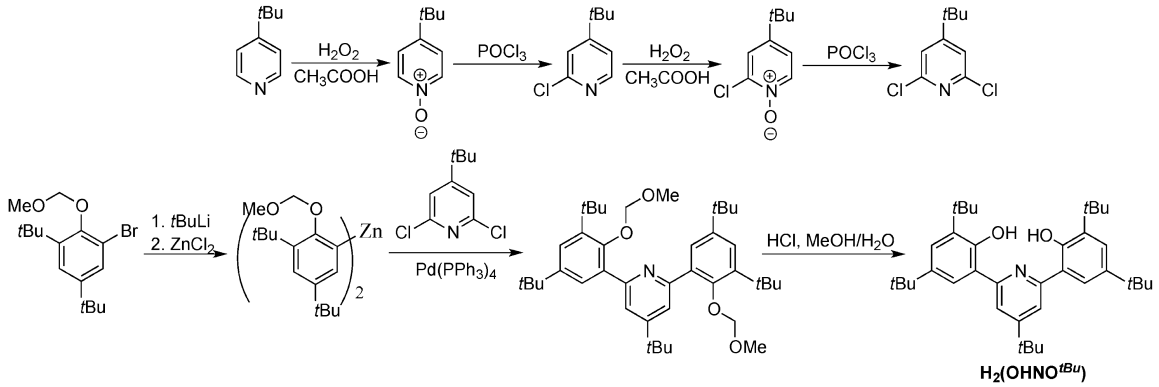

Scheme 2.2. Synthesis of the ligand $H_2(ONO^{tBu})$.

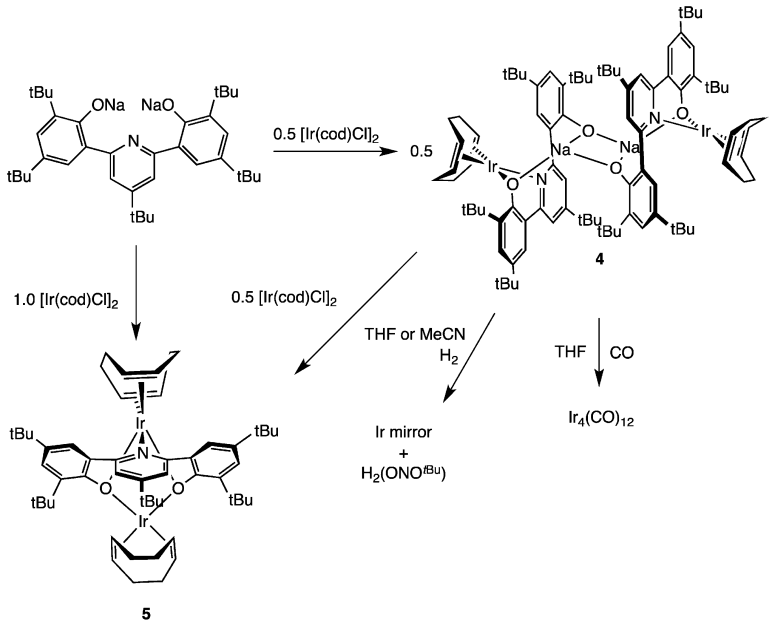

Scheme 2.3. Synthesis and reactivity of $[NaIr(cod)(ONO^{tBu})]_2$, **4**.

Figure 2.3. Crystal structure of **4**. The *tert*-butyl groups and a disordered pentane solvent molecule have been removed for clarity. Selected bond lengths (Å) and angles (°): Ir-O1, 2.0990(1); Ir-N1, 2.1274(1); O1-Na1, 2.2145(1); O2-Na1, 2.1926(1); O2′-Na1, 2.2841(1); O1-Ir-N1, 81.268(3); O1-Na1-O2, 104.799(3); O1-Na1-O2′, 106.989(3); O2-Na1-O2′, 100.484(2).

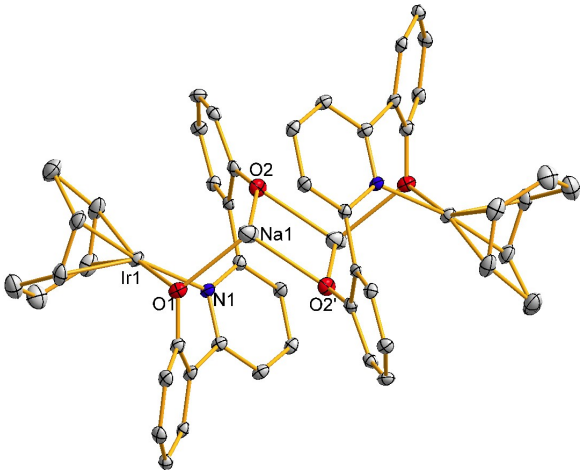

nitrogen of the ligand, while Ir2 is square planar and coordinated only to the two phenolate oxygens (Figure 2.4). (The Ir1-N and Ir2-N distances are 2.07 and 3.00 Å, respectively.)

2.3.2 Synthesis and Characterization of Ir^{III} Complexes

Complex **4** is oxidized by $AgPF_6$ or $[FeCp_2][PF_6]$ in a mixture of THF and acetonitrile to [(ONO^{tBu})-Ir(cod)(MeCN)][PF_6] (**6**, Scheme 2.4), which was isolated as a crystalline product, although it decomposes over time in the presence of excess acetonitrile. Oxidation of **4** with AgOTf in benzene gave the neutral triflate complex (ONO^{tBu})Ir(cod)OTf (**7**). Both complexes exhibit approximately octahedral geometry (Figures 2.5 and 2.6); in solution they behave as strong electrophiles, polymerizing THF and slowly decomposing in other coordinating solvents.

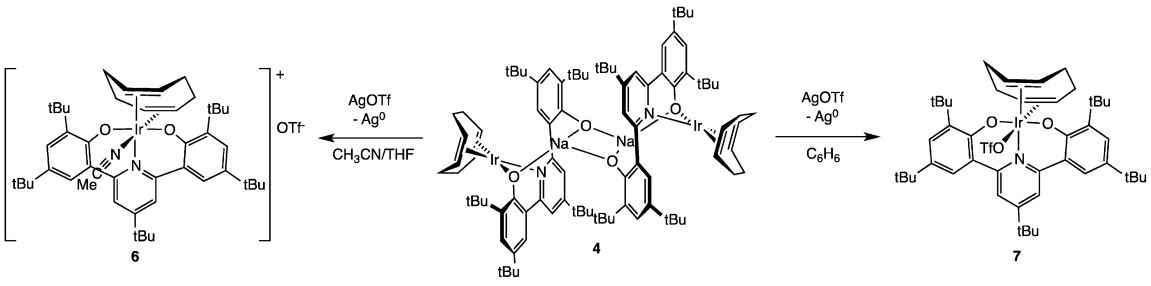

Scheme 2.4. Oxidation of [NaIr(cod)(ONO^{tBu})]$_2$, **4**, to Ir^{III} species.

Treatment of **7** with two equivalents of triphenylphosphine yielded yellow *trans*-(ONO^{tBu})Ir-(PPh_3)$_2$OTf (**8**, Equation 2.1). Attempts to displace cyclooctadiene from **7** with triethylphosphine or

Figure 2.4. Crystal structure of **5**. The *tert*-butyl groups have been removed for clarity. Selected bond lengths (Å) and angles (°): Ir1-O1, 2.2701(1); Ir1-O2, 2.2962(1); Ir1-N1, 2.0818(1); Ir2-O1, 2.0808(1); Ir2-O2, 2.0771(1); Ir2-N1, 2.9953(1); O1-Ir1-O2, 68.864(1); N1-Ir1-O1, 76.957(2); N1-Ir1-O2, 75.747(1); O1-Ir2-O2, 76.775(2); Ir1-O1-Ir2, 103.134(2); Ir1-O2-Ir2, 102.367(2).

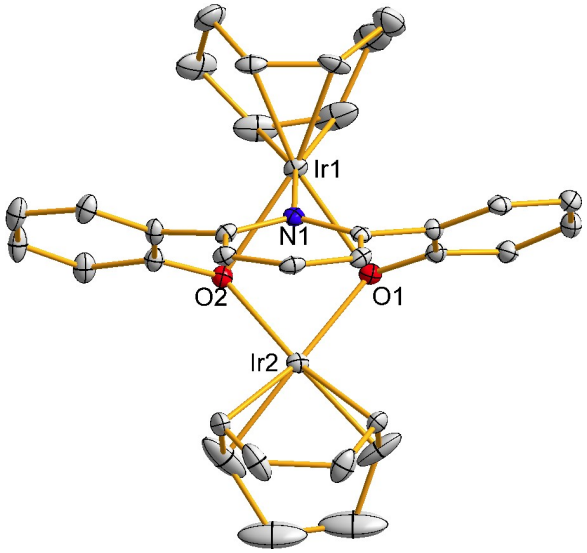

Figure 2.5. Crystal structure of **6**. A benzene solvent molecule and the PF_6 counterion have been removed for clarity. Selected atom distances (Å) and angles (°): Ir1-N1, 2.0736(8); Ir1-N2, 2.0456(8); Ir1-O1, 2.0540(7); Ir1-O2, 2.0849(7); N2-C46, 1.1371(12); O1-Ir1-N1, 85.86(3); O1-Ir1-N2, 81.05(3); O2-Ir1-O1, 89.17(3); O2-Ir1-N2, 85.09(3); O1-Ir1-O2, 165.29(3); N1-Ir1-N2, 89.69(3); Ir1-N2-C46, 173.51(8).

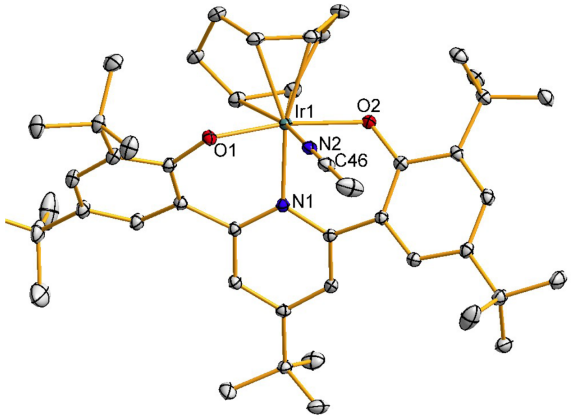

Figure 2.6. Crystal structure of **7**. The two *tert*-butyl groups *ortho* to the phenoxy moieties have been removed for clarity. Selected atom distances (Å) and angles (°): Ir1-O1, 2.0431(6); Ir1-N1, 2.0738(6); Ir1-O2, 2.0836(6); Ir1-O3, 2.1247(6); Ir1-C39, 2.1725(8); Ir1-C40, 2.1865(8); Ir1-C44, 2.2592(8); Ir1-C43, 2.2656(8); O1-Ir1-N1, 84.59(2); O1-Ir1-O2, 163.22(2); N1-Ir1-O2, 88.90(2); O1-Ir1-O3, 80.91(2); N1-Ir1-O3, 87.90(2); O2-Ir1-O3, 83.42(2); O1-Ir1-C39, 121.97(3); N1-Ir1-C39, 95.20(3); O2-Ir1-C39, 73.96(3); O3-Ir1-C39, 157.08(3); O1-Ir1-C40, 84.60(3); N1-Ir1-C40, 90.09(3); O2-Ir1-C40, 110.91(3); O3-Ir1-C40, 165.50(3); C39-Ir1-C40, 37.42(3); O1-Ir1-C44, 110.92(3); N1-Ir1-C44, 164.19(3); O2-Ir1-C44, 75.34(3); O3-Ir1-C44, 91.51(3); C39-Ir1-C44, 79.40(3); C40-Ir1-C44, 94.28(3); O1-Ir1-C43, 77.60(3); N1-Ir1-C43, 159.93(3); O2-Ir1-C43, 110.72(3); O3-Ir1-C43, 98.24(3); C39-Ir1-C43, 86.58(3); C40-Ir1-C43, 79.18(3); C44-Ir1-C43, 35.50(3).

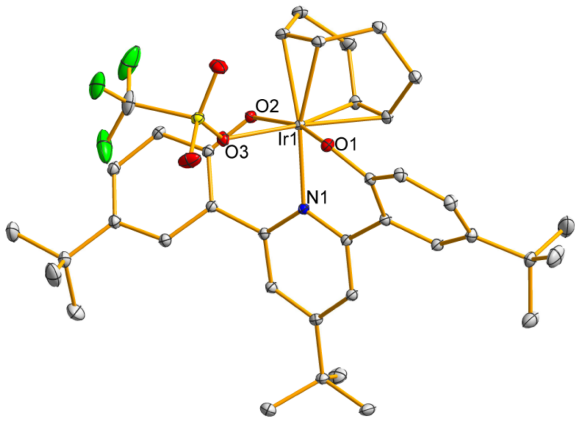

tricyclohexylphosphine led only to decomposition, while the reaction of **7** with tris(*o*-tolyl)phosphine resulted in protonated ligand, perhaps by benzylic C−H activation followed by reductive elimination of phenol. The crystal structure of **8** is show in Figure 2.7.

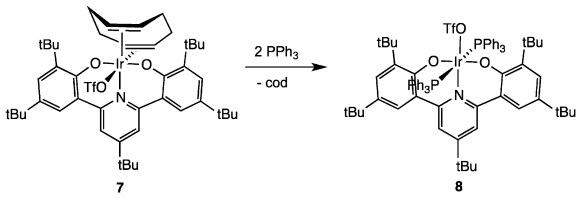

(2.1)

Exposure of **8** to water, followed by addition of proton sponge at room temperature gave *trans*-(ONO^{tBu})Ir(PPh$_3$)$_2$OH (**9**, Equation 2.2). Both **8** and **9** were converted to the corresponding chloride (**10**) by heating at 90°C in dichloromethane for several hours or several days, respectively (Equation 2.3). Formation of **10** from **8** or **9** is much faster in the presence of added tetrabutylammonium chloride. The crystal structure of **9** is show in Figure 2.8.

Figure 2.7. Crystal structure of **8**. Two benzene solvent molecules, a *tert*-butyl group's methyls, and the phosphine ligands' phenyl groups (except *ipso* carbons) have been removed for clarity. Selected atom distances (Å) and angles (°): Ir1-N1, 2.001(3); Ir1-O1, 2.049(2); Ir1-O2, 2.051(2); Ir1-O3, 2.166(2); Ir1-P1, 2.4142(8); Ir1-P2, 2.4165(8); N1-Ir1-O1, 90.68(9); N1-Ir1-O2, 91.55(9); O1-Ir1-O2, 177.70(8); N1-Ir1-O3, 176.28(9); O1-Ir1-O3, 87.33(8); O2-Ir1-O3, 90.41(8); N1-Ir1-P1, 90.90(7); O1-Ir1-P1, 96.69(6); O2-Ir1-P1, 82.71(6); O3-Ir1-P1, 86.22(6); N1-Ir1-P2, 88.06(7); O1-Ir1-P2, 81.27(6); O2-Ir1-P2, 99.37(6); O3-Ir1-P2, 94.74(6); P1-Ir1-P2, 177.70(3).

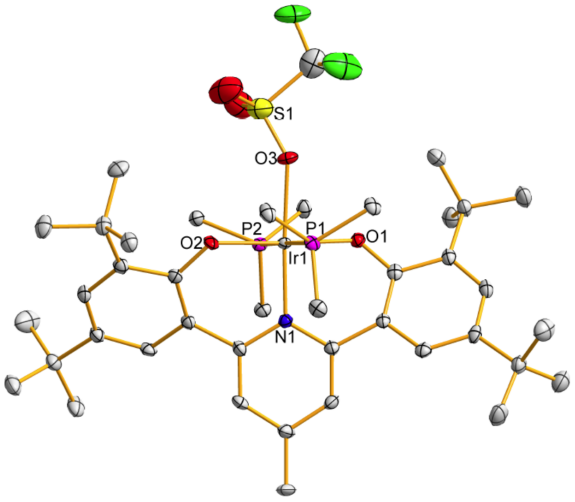

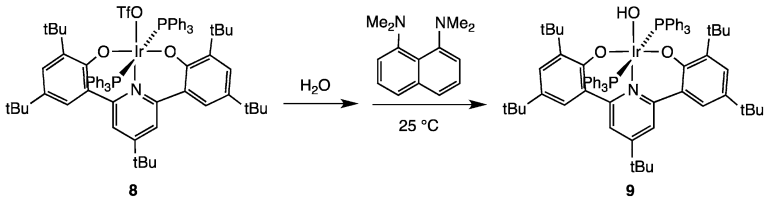

(2.2)

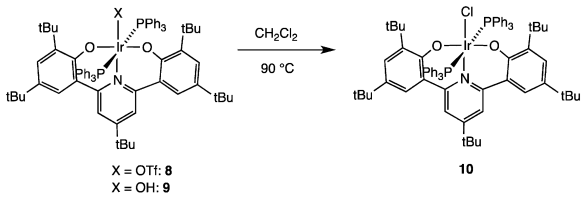

(2.3)

All three complexes (**8**, **9**, and **10**) react with proton sponge to give the hydride (ONO^{tBu})Ir-(PPh$_3$)$_2$H (**11**). The reaction of **8** takes place over several days at room temperature or in an hour at 90°C, while **9** and **10** react more slowly at 90°C. The crystal structure of **11** is show in Figure 2.9.

The proposed mechanism for this transformation is single-electron transfer followed by H-atom abstraction (Scheme 2.5); the oxidized proton sponge byproduct shown was observed (quantitatively)

Figure 2.8. Crystal structure of **9**. The *tert*-butyl groups have been removed for clarity. Selected atom distances (Å) and angles (°): Ir1-N1, 2.0395(14); Ir1-O3, 2.0561(13); Ir1-O1, 2.0624(11); Ir1-O2, 2.0686(11); Ir1-P1, 2.3654(5); Ir1-P2, 2.3920(5); N1-Ir1-O3, 179.30(6); N1-Ir1-O1, 89.78(5); O3-Ir1-O1, 90.03(5); N1-Ir1-O2, 89.99(5); O3-Ir1-O2, 90.22(5); O1-Ir1-O2, 178.69(5); N1-Ir1-P1, 97.67(4); O3-Ir1-P1, 83.02(4); O1-Ir1-P1, 95.33(4); O2-Ir1-P1, 83.43(4); N1-Ir1-P2, 90.84(4); O3-Ir1-P2, 88.46(4); O1-Ir1-P2, 81.46(4); O2-Ir1-P2, 99.83(4); P1-Ir1-P2, 170.911(15).

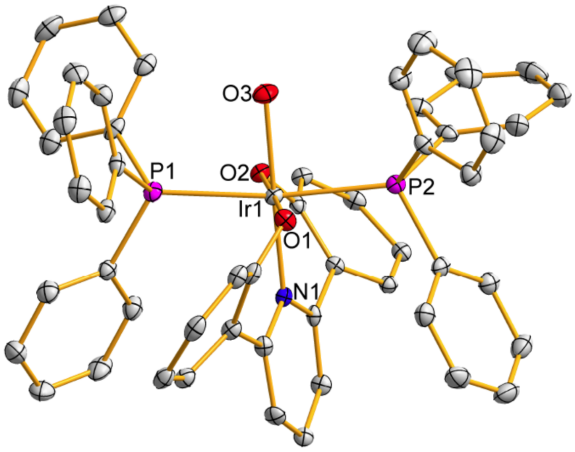

Figure 2.9. Crystal structure of **11**. A pentane solvent molecule and the *tert*-butyl groups have been removed for clarity. Selected atom distances (Å) and angles (°): Ir1-O1, 2.0663(11); Ir1-O2, 2.0764(11); Ir1-N1, 2.1020(16); Ir1-P2, 2.3229(5); Ir1-P1, 2.3320(5); Ir1-H1, 1.70(2); O1-Ir1-O2, 176.19(5); O1-Ir1-N1, 87.97(5); O2-Ir1-N1, 88.25(5); O1-Ir1-P2, 86.17(4); O2-Ir1-P2, 94.68(3); N1-Ir1-P2, 95.82(4); O1-Ir1-P1, 96.13(4); O2-Ir1-P1, 83.91(3); N1-Ir1-P1, 97.67(4); P2-Ir1-P1, 166.384(19); O1-Ir1-H1, 95.6(6); O2-Ir1-H1, 88.2(6); N1-Ir1-H1, 176.3(7); P2-Ir1-H1, 85.7(7); P1-Ir1-H1, 80.7(7).

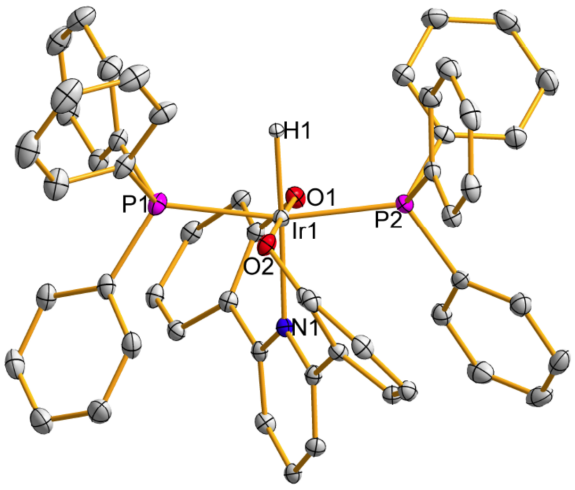

by NMR. A related reaction of proton sponge with an Ir^{III} complex has previously been reported [11]. In further support of this proposal, **11** was also obtained by treatment of **8** with cobaltocene (a one-electron donor) and the H atom donor 9,10-dihydroanthracene (DHA), or by heating **8** with sodium hydride. **11** can also be obtained from the reaction of **8** with lithium methoxide or diethylzinc, presumably *via* β-hydride elimination from an iridium-methoxy [12] or iridium-ethyl intermediate, respectively. The two latter routes give **11** most cleanly; in the reactions with proton sponge, we were unable to separate **11** from the byproducts.

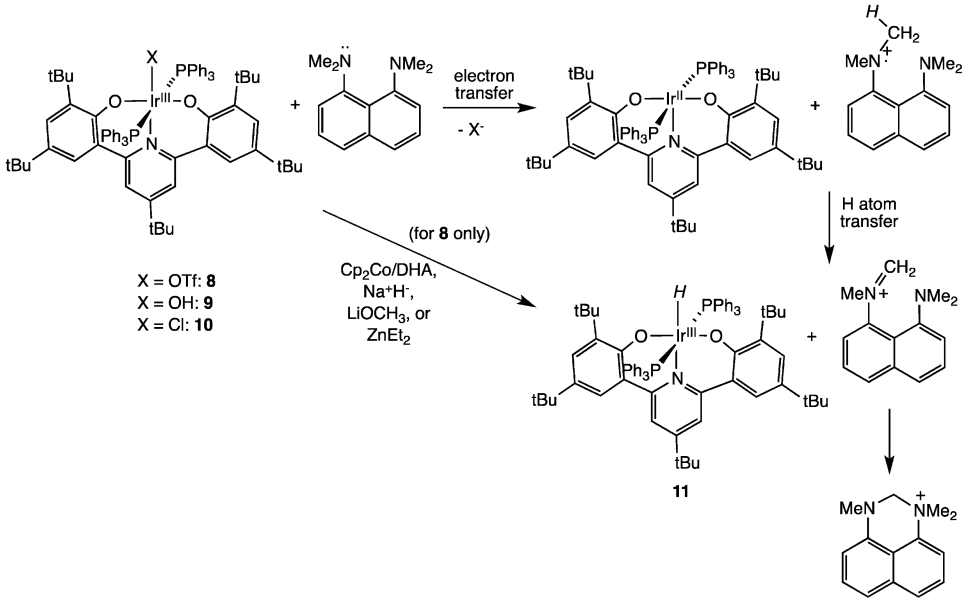

Scheme 2.5. Synthetic routes to $(ONO^{tBu})Ir(PPh_3)_2H$, **11**.

Treatment of **8** with dimethylzinc yielded the water-stable methyl complex $(ONO^{tBu})Ir(PPh_3)_2Me$ (**12**). Oxidation of **12** with I_2 yields the iodide $(ONO^{tBu})Ir(PPh_3)_2I$ (**13**) and methyl iodide (Scheme 2.6).

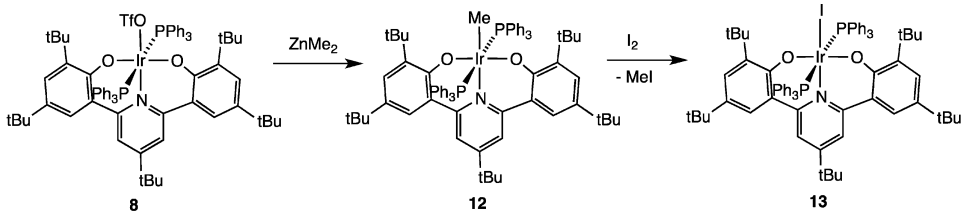

Scheme 2.6. Methylation to $(ONO^{tBu})Ir(PPh_3)_2Me$, **12**, and subsequent functionalization with I_2 to $(ONO^{tBu})Ir(PPh_3)_2I$, **13**.

Crystal structures for complexes **8**, **9**, **11**, **12**, and **13** all exhibit closely analogous octahedral geometries. The structures of **12** and **13** are shown in Figures 2.10 and 2.11.

Unlike **8**, **12** reacts cleanly with triethylphosphine to give the analogous PEt_3 complex (**14**,

Figure 2.10. Crystal structure of **12**. Only *ipso* carbon atoms of the phenyl groups on phosphorus are shown. Selected atom distances (Å) and angles (°): Ir-O1, 2.0901(1); Ir-O2, 2.0700(1); Ir-C74, 2.0952(1); Ir-N, 2.1042(1); Ir-P1, 2.3449(1); Ir-P2, 2.3895(1); O1-Ir-O2, 176.495(3); P1-Ir-P2, 172.872(2); N-Ir-C74, 175.671(3); C74-Ir-O1, 95.588(2); C74-Ir-O2, 87.799(2); C74-Ir-P1, 85.584(2); C74-Ir-P2, 87.309(2); O1-Ir-P1, 82.692(2); O1-Ir-P2, 98.559(2); O2-Ir-P1, 96.698(2); O2-Ir-P2, 82.473(2); N-Ir-O1, 88.429(2); N-Ir-O2, 88.212(2); N-Ir-P1, 96.553(2); N-Ir-P2, 90.503(2).

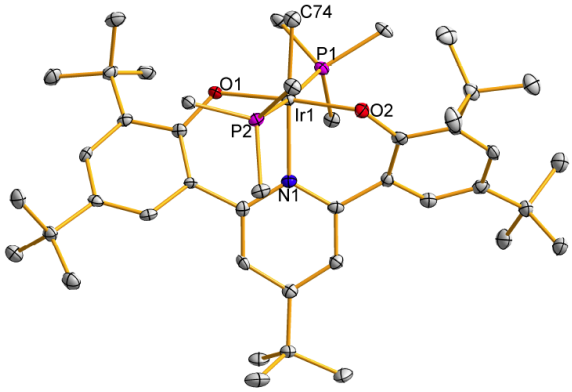

Figure 2.11. Crystal structure of **13**. Two pentane solvent molecules and the *tert*-butyl groups have been removed for clarity. Selected atom distances (Å) and angles (°): Ir1-N1, 2.040(3); Ir1-O2, 2.066(2); Ir1-O1, 2.076(2); Ir1-P2, 2.4233(10); Ir1-P1, 2.4247(11); Ir1-I2, 2.7013(3); N1-Ir1-O2, 89.52(10); N1-Ir1-O1, 88.88(10); O2-Ir1-O1, 178.36(9); N1-Ir1-P2, 89.69(9); O2-Ir1-P2, 78.59(8); O1-Ir1-P2, 101.03(8); N1-Ir1-P1, 89.04(9); O2-Ir1-P1, 102.10(8); O1-Ir1-P1, 78.25(8); P2-Ir1-P1, 178.55(3); N1-Ir1-I2, 179.19(9); O2-Ir1-I2, 90.56(6); O1-Ir1-I2, 91.05(7); P2-Ir1-I2, 91.12(2); P1-Ir1-I2, 90.15(2).

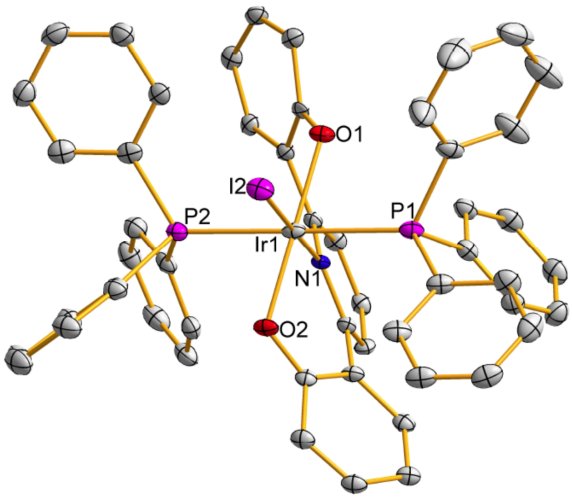

Scheme 2.7). **14** appears to be more thermally stable than **12**, only slowly decomposing at temperatures above 120°C. It reacts similarly with I_2, giving methyl iodide and (ONO^{tBu})Ir(PEt$_3$)$_2$I (**15**). Both **14** (Figure 2.12) and **15** (Figure 2.13) were characterized crystallographically. Iodide complex **15** is unstable in methylene chloride, converting to the analogous chloride over several days at room temperature. Such behavior was not observed with the PPh_3 analogue **13**.

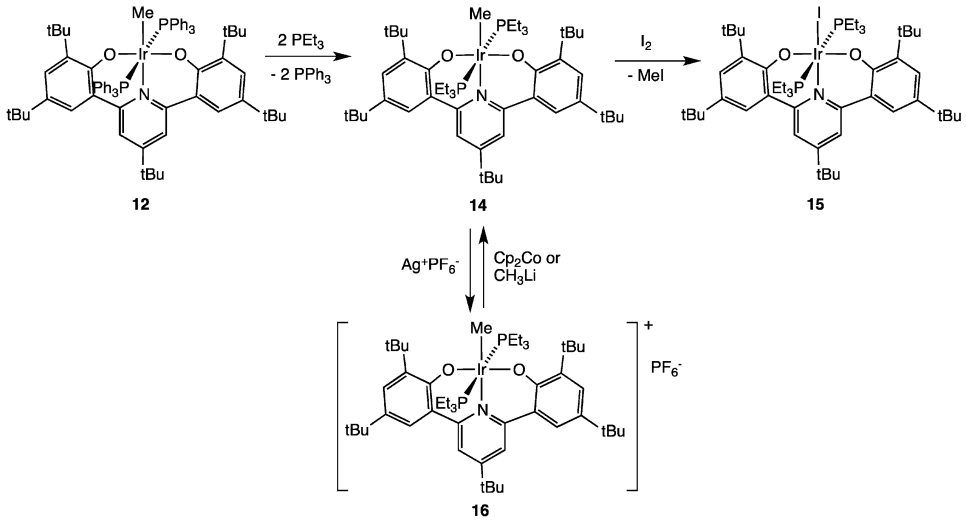

Scheme 2.7. Synthesis of (ONO^{tBu}Ir(PEt$_3$)$_2$ complexes.

Figure 2.12. Crystal structure of **14**. The ethyl groups of one phosphine ligand have been removed for clarity. Selected atom distances (Å) and angles (°): Ir1-O2, 2.0674(11); Ir1-O1, 2.0702(11); Ir1-N1, 2.1050(14); Ir1-C50, 2.1154(17); Ir1-P2, 2.3479(5); Ir1-P1, 2.3514(5); O2-Ir1-O1, 178.26(5); O2-Ir1-N1, 88.65(5); O1-Ir1-N1, 89.83(5); O2-Ir1-C50, 91.12(6); O1-Ir1-C50, 90.42(6); N1-Ir1-C50, 178.40(6); O2-Ir1-P2, 84.03(4); O1-Ir1-P2, 95.23(4); N1-Ir1-P2, 93.93(4); C50-Ir1-P2, 87.61(5); O2-Ir1-P1, 97.78(4); O1-Ir1-P1, 83.10(4); N1-Ir1-P1, 91.40(4); C50-Ir1-P1, 87.07(5); P2-Ir1-P1, 174.416(16).

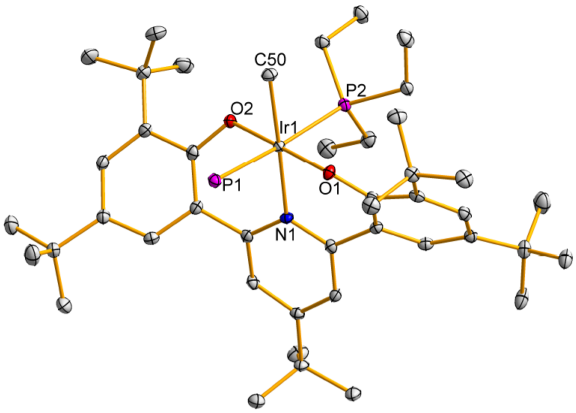

In both I_2 oxidations a dark blue color is observed over much of the course of the reaction, even though the starting complexes and the products are all yellow. Cyclic voltammetry experiments show quasi-reversible oxidations at 20 and 780 mV for **12** and reversible oxidations at −100 and

Figure 2.13. Crystal structure of **15**. The ethyl groups of the phosphine ligands have been removed for clarity. Selected atom distances (Å) and angles (°): Ir1-N1, 2.0619(13); Ir1-O2, 2.0648(11); Ir1-O1, 2.0661(11); Ir1-C(50), 2.148(7); Ir1-P1, 2.3711(4); Ir1-P2, 2.3722(4); Ir1-I2, 2.6625(3); N1-Ir1-O2, 89.86(5); N1-Ir1-O1, 88.67(5); O2-Ir1-O1, 178.36(5); N1-Ir1-C(50), 177.12(15); O2-Ir1-C(50), 89.65(17); O1-Ir1-C(50), 91.86(17); N1-Ir1-P1, 93.81(4); O2-Ir1-P1, 95.64(3); O1-Ir1-P1, 83.74(3); C(50)-Ir1-P1, 89.06(15); N1-Ir1-P2, 91.30(4); O2-Ir1-P2, 82.36(3); O1-Ir1-P2, 98.40(3); C(5)-Ir1-P2, 85.82(15); P1-Ir1-P2, 174.510(14); N1-Ir1-I2, 178.40(4); O2-Ir1-I2, 91.65(3); O1-Ir1-I2, 89.83(3); C(50)-Ir1-I2, 3.05(16); P1-Ir1-I2, 86.571(11); P2-Ir1-I2, 88.374(11).

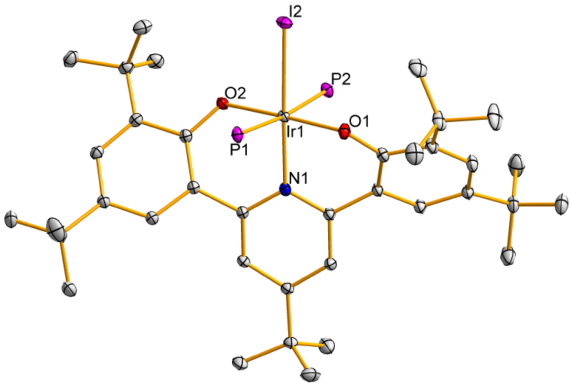

840 mV for **14** both *vs.* ferrocene (Figure 2.14). The reaction of **14** with $AgPF_6$ gave dark blue $[(ONO^{tBu})Ir(PEt_3)_2Me]PF_6$ (**16**, Scheme 2.7), characterized by a crystal structure and an EPR spectrum (Figure 2.15) that are very similar to those of the (relatively few) organometallic Ir^{IV} species reported [13]. **16** could be reduced back to **14** with either cobaltocene or methyllithium; furthermore, treatment of **16** with tetrabutylammonium iodide gave MeI and some **15**. All of this suggests that the reaction of **14** (or **12**) with I_2 begins with a single electron transfer to generate an intermediate cationic Ir^{IV} -Me species, which undergoes S_N2 attack by I^- at the Ir−C bond. The CV data suggest that further oxidization of **16** might be possible, perhaps even to an Ir^V-methyl complex, but no such species has yet been isolated or otherwise identified. (The close similarity of the second potentials, in contrast to the first, may indicate that the second wave corresponds to oxidation of the ONO^{tBu} ligand rather than at Ir.) The crystal structure of **16** is show in Figure 2.16).

2.3.3 C−H Activation by $Ir^{III}(ONO^{tBu})$ Complexes

In benzene solution, $(ONO^{tBu})Ir(PPh_3)_2Me$ converts over the course of several hours at 65°C to the analogous phenyl complex $(ONO^{tBu})Ir(PPh_3)_2Ph$ (**17**), with evolution of methane. The benzene solution of **17** reacts further over the course of several weeks at 65°C to give a cyclometalated product, $(ONO^{tBu})Ir(PPh_3)[\kappa^2\text{-}PPh_2(o\text{-}C_6H_4)]$ (**18**, Equation 2.4).

Figure 2.14. Cyclic voltammetry of **14**, carried out in the air at room temperature. The solvent was dichloromethane with 0.1 M tetrabutylammonium tetrafluoroborate added as the electrolyte. Multiple runs were made with scan rates from 50 to 400 mV/s. Quasi-reversibility is seen in the form of a following chemical step. The dip at 0.3 V is an artifact.

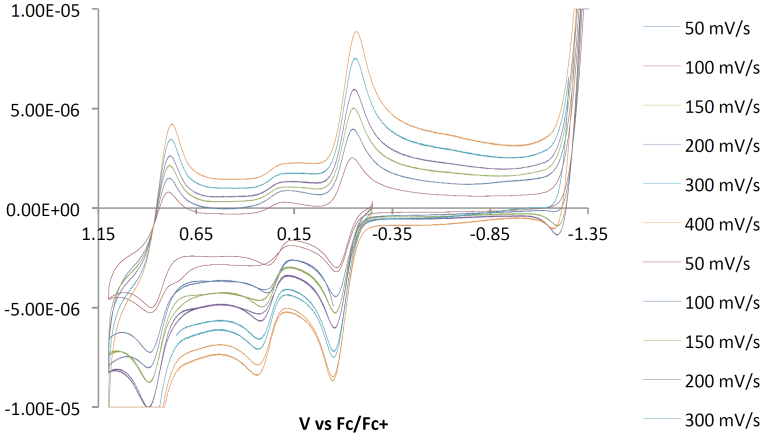

Figure 2.15. EPR spectrum of $[(ONO^{tBu})Ir(PEt_3)_2Me]PF_6$, **16**, in dichloromethane at 20 K.

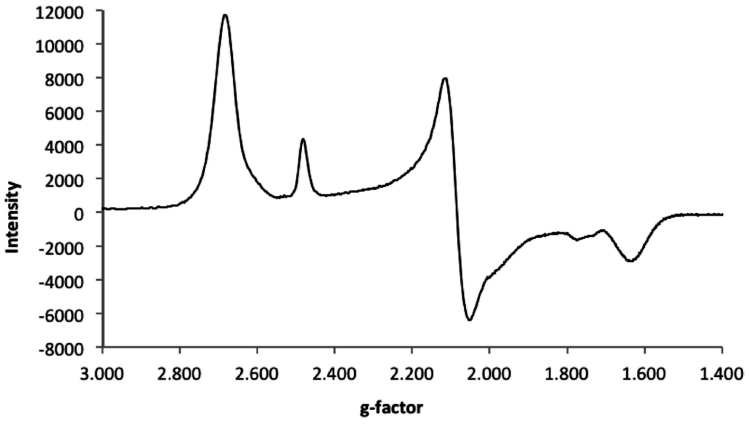

Figure 2.16. Crystal structure of one of the molecules of **16** in the unit cell. The unit cell has four iridium-containing molecules total; this figure only shows one of them. In addition, ethyl groups on the phosphine ligands, as well as the six benzene molecules per unit cell, have been removed for clarity. Selected atom distances (Å) and angles (°): Ir1-O2A, 1.994(5); Ir1-O1A, 2.011(5); Ir1-C50A, 2.101(8); Ir1-N1A, 2.129(7); Ir1-P2A, 2.400(2); Ir1-P1A, 2.418(2); O2A-Ir1-O1A, 173.5(2); O2A-Ir1-C50A, 94.2(3); O1A-Ir1-C50A, 92.3(3); O2A-Ir1-N1A, 87.4(2); O1A-Ir1-N1A, 86.1(2); C50A-Ir1-N1A, 177.4(3); O2A-Ir1-P2A, 82.62(17); O1A-Ir1-P2A, 98.06(18); C50A-Ir1-P2A, 84.4(2); N1A-Ir1-P2A, 93.78(18); O2A-Ir1-P1A, 98.16(17); O1A-Ir1-P1A, 81.81(18); C50A-Ir1-P1A, 89.8(2); N1A-Ir1-P1A, 91.96(18); P2A-Ir1-P1A, 174.24(8).

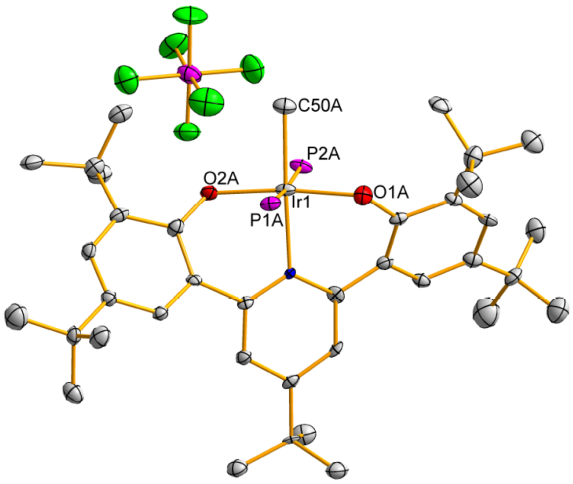

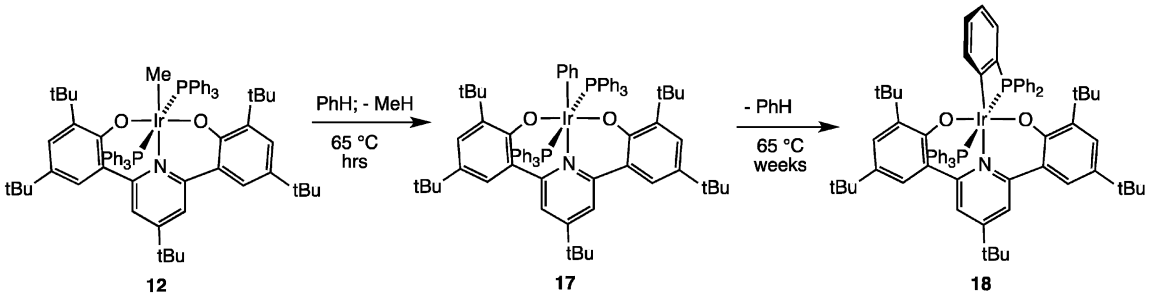

(2.4)

When **17** is isolated, redissolved in a solvent other than benzene (such as *p*-xylene), and heated to 65°C, conversion to **18** is complete within a few days. Both **17** (Figure 2.17 and **18** (Figure 2.18) were characterized crystallographically.

Thermolysis of **12** in C_6D_6 yields CH_4 as the only detectable methane isotopologue, and mass spectrometry of the resulting isolated phenyl product **17** shows incorporation of six D atoms (Equation 2.5). In contrast, heating $(ONO^{tBu})Ir[P(C_6D_5)_3]_2(CH_3)$ (**12**-d_{30}) in C_6D_6 yields only CH_3D; this reaction is slower than that of all-protio-**12**, exhibiting a KIE of **4** 2.20. The PEt_3 analogue **14** reacts very slowly in C_6H_6 or C_6D_6, requiring several weeks at 120°C to give $(ONO^{tBu})Ir(PEt_3)_2Ph$ and CH_4 or CH_3D, respectively.

Figure 2.17. Crystal structure of **17**. A benzene and a pentane solvent molecule, as well as the phosphine phenyl groups, have been removed for clarity. The molecule is symmetric about the iridium center. Selected atom distances (Å) and angles (°): Ir1-O1, 2.0744(12); Ir1-C40, 2.074(3); Ir1-N1, 2.103(2); Ir1-P1, 2.3921(6); O1-Ir1-C40, 90.05(4); O1-Ir1-O1′, 179.91(8); C40-Ir1-O1′, 90.04(4); O1-Ir1-N1, 89.95(4); C40-Ir1-N1, 180.0; O1′-Ir1-N1, 89.96(4); O1-Ir1-P1′, 97.70(4); C40-Ir1-P1′, 88.831(13); O1′-Ir1-P1′, 82.30(4); N1-Ir1-P1′, 91.169(13); O1-Ir1-P1, 82.30(4); C40-Ir1-P1, 88.829(13); O1′-Ir1-P1, 97.70(4); N1-Ir1-P1, 91.171(13); P1′-Ir1-P1; 177.66(3).

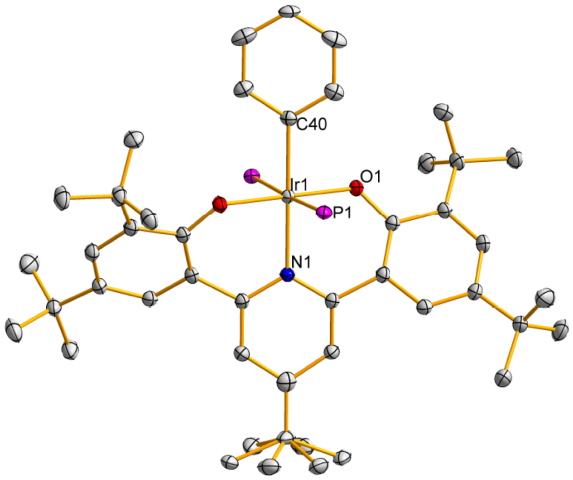

Figure 2.18. Crystal structure of **18**. A dodecane solvent molecule and parts of several phenyl and *tert*-butyl groups have been removed for clarity. Selected atom distances (Å) and angles (°): Ir-O1, 2.0696(1); Ir-O2, 2.0612(1); Ir-C46, 2.0669(1); Ir-N, 2.1156(1); Ir-P4, 2.3462(1); Ir-P5, 2.3483(1); O1-Ir-O2, 174.874(3); P4-Ir-P5, 164.008(2); N-Ir-C46, 167.055(4); C46-Ir-O1, 100.779(3); C46-Ir-O2, 80.655(3); C46-Ir-P4, 95.708(2); C46-Ir-P5, 68.499(2); O1-Ir-P4, 85.316(3); O1-Ir-P5, 94.944(2); O2-Ir-P4, 99.475(2); O2-Ir-P5, 80.959(3); N-Ir-O1, 88.656(3); N-Ir-O2, 89.198(3); N-Ir-P4, 93.867(3); N-Ir-P5, 102.125(3).

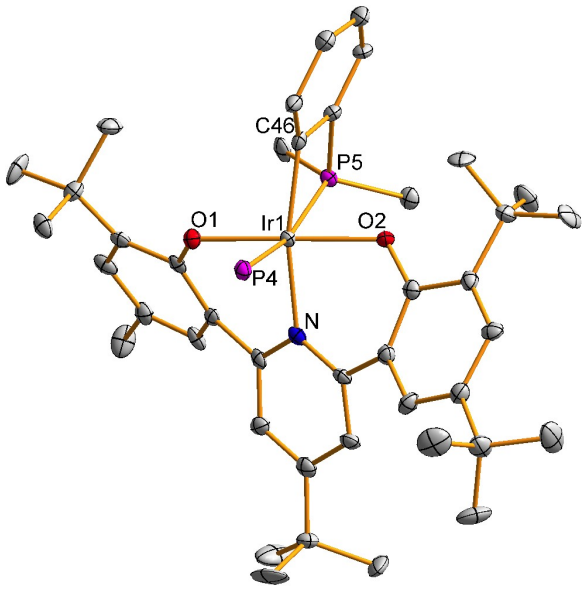

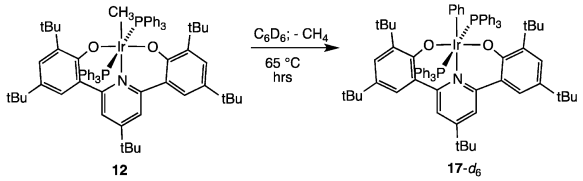

(2.5)

Thermolysis of **12** at 65°C in methylene chloride, THF, ether, or *p*-xylene leads directly to **18** (Equation 2.6). These transformations require less than one day for complete conversion (in methylene chloride or *p*-xylene), comparable to the time needed for conversion of **12** to **17** and much faster than the conversion of **17** to **18** in benzene. Reaction of **12** in toluene at 65°C proceeds similarly to that in benzene; although a single pure compound could not be isolated, the mass spectrum of the mixture is consistent with formation of an Ir^{III} tolyl compound, $(ONO^{tBu})Ir(PPh_3)_2(C_6H_4CH_3)$. The ^{31}P NMR shows two strong signals of roughly equal intensity with shifts close to that of phenyl compound **17**, suggesting the formation of two isomers, presumably *meta* and *para* (since *p*-xylene is unreactive); a much weaker nearby signal may indicate a small amount of the *ortho* isomer.

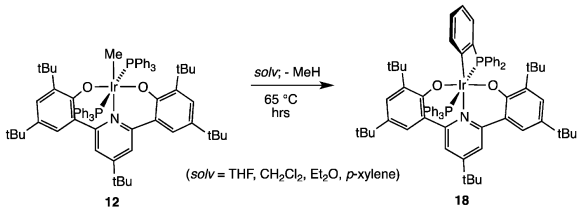

(2.6)

Although **12** is insoluble in acetonitrile, thermolysis in methylene chloride containing a small amount of acetonitrile affords a mixture of **18** and a product resulting from C−H activation of acetonitrile, $[(ONO^{tBu})Ir(PPh_3)(CH_2CN)]_2$ (**19**); with CD_3CN, CH_4 is the only methane isotopologue produced (Equation 2.7). **19** has the dimeric structure shown in Figure 2.19, where coordination of N from the (CH_2CN) group bonded to each Ir has displaced a PPh_3 ligand from the other. Although two ^1H NMR signals would be expected for the (CH_2CN) methylene protons, which are diastereotopic in the solid-state structure, only one is observed; this could result from either accidental degeneracy or dissociation of the dimeric structure in solution.

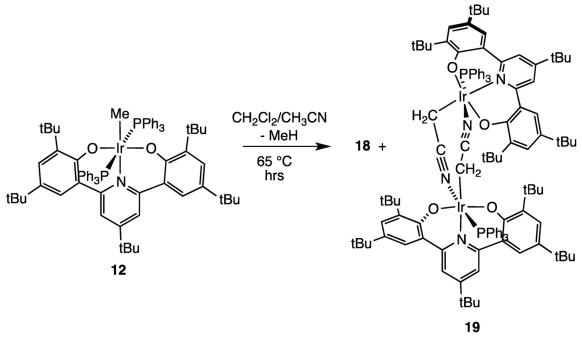

(2.7)

Figure 2.19. Crystal structure of **19** [14]. A benzene solvent molecule, phosphine phenyl, and (ONO) *tert*-butyl groups have been removed for clarity. Selected atom distances (Å) and angles (°): Ir1-O1, 2.0190(2); Ir1-O2, 2.0883(2); Ir1-C104, 2.1472(2); Ir1-N1, 2.0758(2); Ir1-N4, 2.0882(2); Ir1-P1, 2.2654(2); N3-C103, 1.1271(1); C103-C104, 1.4380(1); N4-C102, 1.1278(1); C102-C101, 1.4482(2); Ir2-O3, 2.0912(2); Ir2-O4, 2.0396(2); Ir2-C101, 2.1740(3); Ir2-N2, 2.0854(3); Ir2-N3, 2.1290(2); Ir2-P2, 2.2574(2); O1-Ir1-O2, 173.203(10); N4-Ir1-P1, 173.670(9); N1-Ir1-C104, 170.591(10); C104-Ir1-O1, 81.941(8); C104-Ir1-O2, 98.236(8); C104-Ir1-N4, 86.476(8); C104-Ir1-P1, 90.036(7); O1-Ir1-N4, 88.426(8); O1-Ir1-P1, 96.321(8); O2-Ir1-N4, 84.807(8); O2-Ir1-P1, 90.475(8); N1-Ir1-O1, 89.793(8); N1-Ir1-O2, 89.439(8); N1-Ir1-N4, 88.823(8); N1-Ir1-P1, 95.360(8); Ir1-N4-C102, 156.881(14); N4-C102-C101, 171.704(16); C102-C101-Ir2, 104.11(1); Ir2-N3-C103, 156.797(13); N3-C103-C104, 172.115(16); C103-C104-Ir1, 105.731(10); O3-Ir2-O4, 174.306(10); N3-Ir2-P2, 171.891(9); N2-Ir2-C101, 172.156(10); C101-Ir2-O3, 96.853(8); C101-Ir2-O4, 84.460(8); C101-Ir2-N3, 85.543(7); C101-Ir2-P2, 88.633(7); O3-Ir2-N3, 85.175(8); O3-Ir2-P2, 89.930(7); O4-Ir2-N3, 89.412(8); O4-Ir2-P2, 95.646(8); N2-Ir2-O3, 89.263(8); N2-Ir2-O4, 88.981(8); N2-Ir2-N3, 90.101(8); N2-Ir2-P2, 96.309(8).

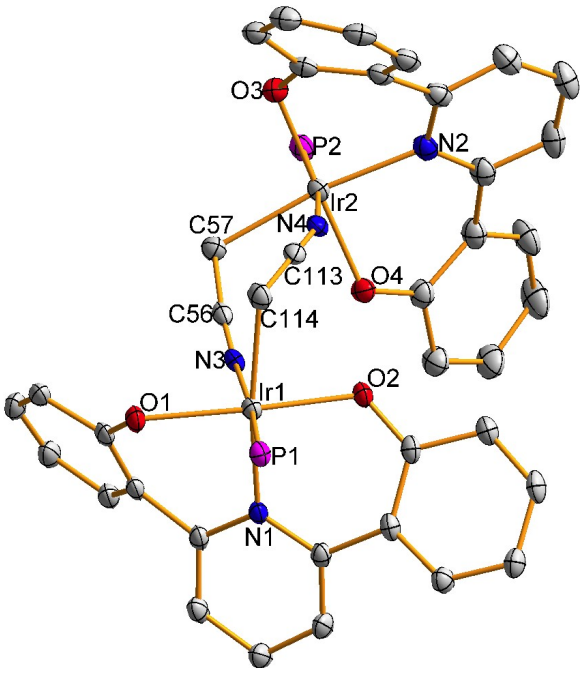

A plausible mechanism for the chemistry of **12** in benzene is shown in Scheme 2.8. The sequence of product formation (**17** and **18** being preferred kinetically and thermodynamically, respectively [15]) would seem to suggest that the first C−H activation is the intermolecular reaction with benzene. But that is excluded by the isotopic labeling results. The H atom that departs with methane clearly comes from a PPh_3 ligand, not solvent benzene, so PPh_3 must be the site of the first C−H activation, even though the corresponding product **18** does not appear at all until much later. We propose therefore that dissociation of one PPh_3 ligand gives coordinatively unsaturated **A**, followed by intramolecular C−H activation and loss of methane to generate cyclometalated intermediate C. In benzene solution coordination of PPh_3 to **C** is not competitive; instead **C** reacts with benzene to give **17** as initial observed product. Subsequent conversion to the thermodynamic product **18** is much slower.

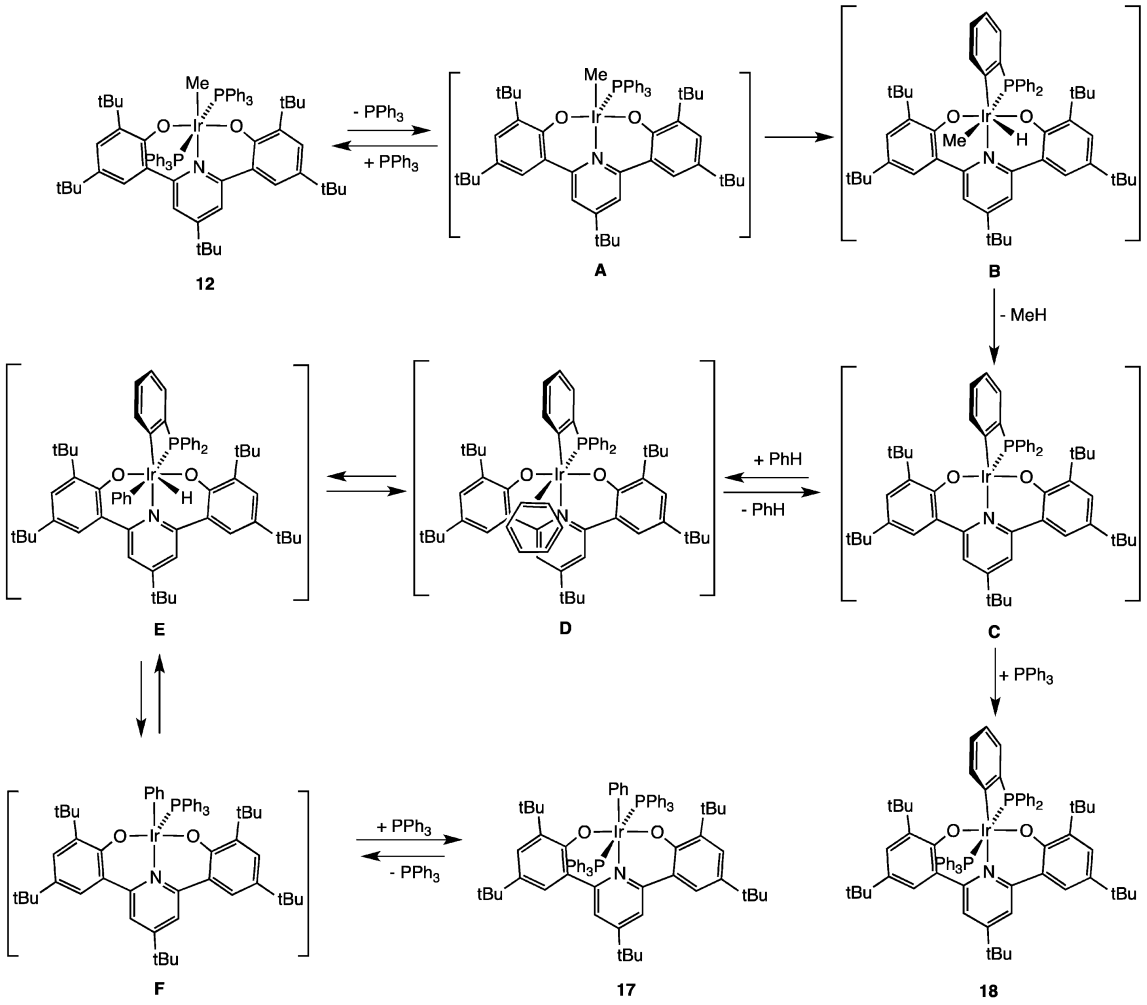

Scheme 2.8. Proposed mechanism for the transformation of **12** in benzene to the kinetic product **17** and the thermodynamic product **18**.

C−H activation is shown in Scheme 2.8 as proceeding *via* oxidative addition to give an Ir^V intermediate, a mechanism that has been supported by both experiment [16] and calculations [17] for the above-mentioned [15] Cp* system. It seems reasonable that similar considerations would apply here as well; but an alternative pathway, such as σ-bond metathesis, cannot be excluded. In any case, conversion of **A** to **C** must be irreversible, as no multiple H/D exchange is observed, whereas conversion of **C** to **F** must be reversible, since **17** eventually reverts to **18**.

The fact that products are obtained from solvent activation with toluene but not *p*-xylene suggests that C−H activation *ortho* to a methyl substituent is sterically inhibited. As a consequence, in the latter solvent **C** (or a π-arene adduct analogous to **D**) has no alternative but to bind PPh_3 and **18** forms directly, as it does in solvents (dichloromethane, ether, THF) that are not susceptible to C−H activation at all. In acetonitrile the two pathways are competitive. The reaction of **14** is much slower, presumably because PEt_3 dissociates much less readily, and leads only to a phenyl product, indicating that cyclometalation of PEt_3 does not take place.

2.3.4 Kinetics of C−H Activation

The transformation of **12** to **17** and/or **18** is readily followed by ^{31}P NMR, as each of the species has a distinct spectrum. In early experiments results were not always highly reproducible; most probably this is due to oxidation of small amounts of PPh_3 by adventitious impurities, which could effect significant acceleration; indeed, deliberate addition of oxidants such as chloranil and dioxygen did speed up conversion of **12** considerably. However, reasonably reproducible rates ($\pm$15%) could be achieved by careful attention to purification of starting complex and solvent as well as exclusion of air.

The somewhat simplified mechanism shown in Scheme 2.9 may be used for analysis; it leaves out the (unobserved) intermediates **B** (which will rapidly convert to **C**) and **D** and **E** (which are presumed to be in rapid equilibrium with **C** and **F**); none of these should have any kinetic consequences. Three transformations will be considered in turn: (1) conversion of **12** to **17** in benzene; (2) conversion of **12** to **18** in *p*-xylene; and (3) conversion of **17** to **18** in benzene or *p*-xylene.

The first of these may be analyzed in terms of reversible dissociation of PPh_3 (henceforth abbreviated as L) followed by rate-determining C−H activation (the k_2 step). Since the conversion of **A** to **C** is irreversible (*vide supra*), no buildup of any intermediate is observed, and formation of **17** is essentially complete before any **18** is observed. In this simplified framework, we can treat the dissociation of L from **12** as a fast pre-equilibrium and the intramolecular C−H activation of L as rate-determining, giving us $K_1 = [\mathbf{A}][\mathrm{L}]/[\mathbf{12}]$. Thus the rate law would be $-d[\mathbf{12}]/dt = d[\mathbf{17}]/dt = k2[\mathbf{A}] = (k_2K_1[\mathbf{12}])/[\mathrm{L}]$, and the rate should be cleanly first order in **12** and inverse-first-order in L. There is a potential complication if no extra L is added: [L] will be governed by both K_1 and K_4, so if these two equilibrium constants were significantly different, [L] would vary

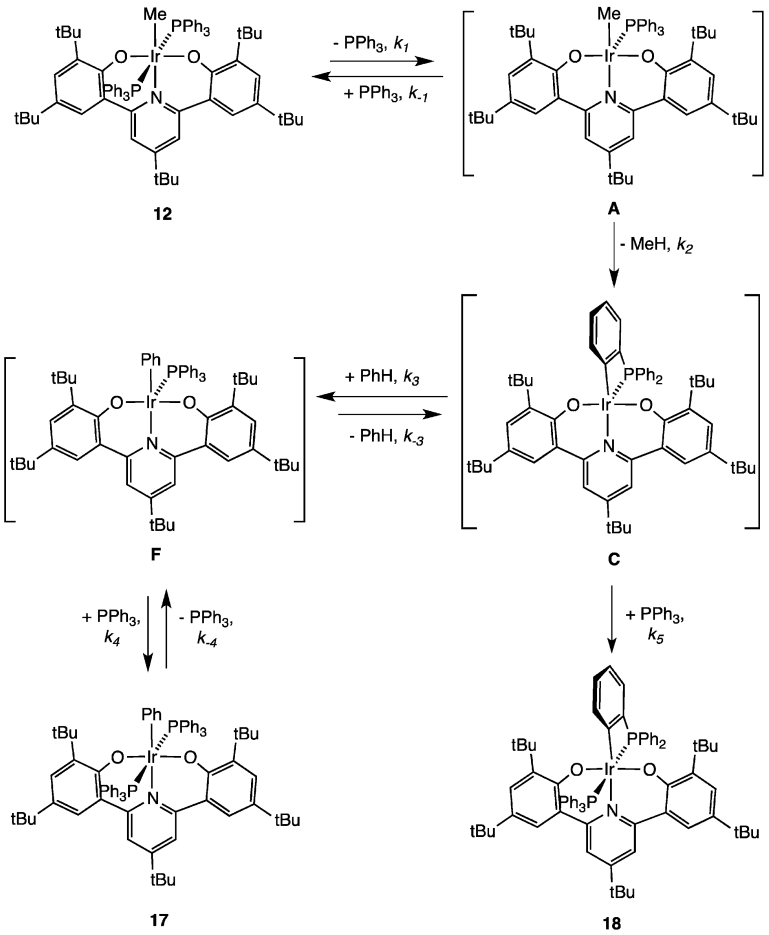

Scheme 2.9. Simplified version of Scheme 2.8, used for kinetic analysis.

in a complex manner as conversion of **12** to **17** proceeds, and the disappearance of **12** or appearance of **17** might not follow clean first-order kinetics. Nonetheless, it does: a good exponential fit is achieved (Figure 2.20, left), with $k_{\text{obs}} = 1.8(3) \times 10^{-4}$ s^{-1} (equivalent to a half-life of about an hour), so any difference in K values is small enough to neglect. The **12**-d_{30} ((ONO$^{t\text{Bu}}$)Ir[P(C$_6$D$_5$)$_3$]$_2$Me) isotopologue behaves similarly, yielding $k_{\text{obs}} = 4.4(6) \times 10^{-5}$ s^{-1} and hence KIE = 4(1) (Figure 2.20, right), consistent with the assignment of C−H activation of L as rate-determining.

Figure 2.20. Left: kinetics of conversion of **12** to **17** in C_6D_6 at 65°C. Right: kinetics of conversion of **12**-d_{30} ((ONO$^{t\text{Bu}}$)Ir[P(C$_6$D$_5$)$_3$]$_2$Me) to **17**-d_{36} ((ONO$^{t\text{Bu}}$)Ir[P(C$_6$D$_5$)$_3$]$_2$C$_6$D$_5$) in C_6D_6 at 65°C.

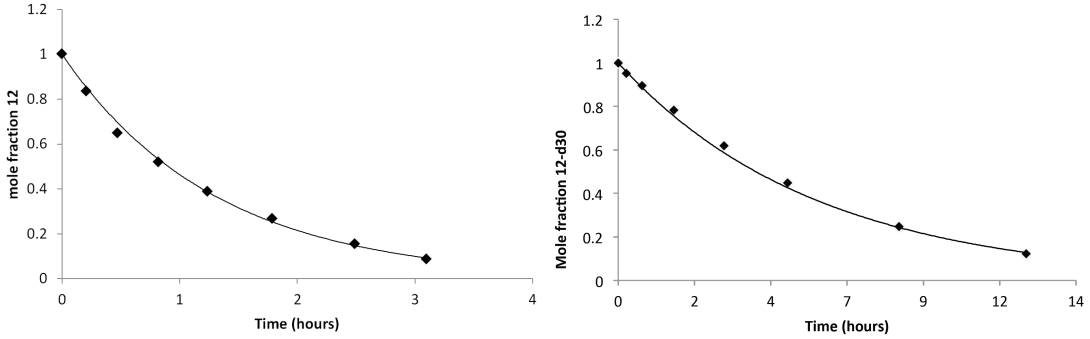

As expected, the addition of extra L slows the reaction significantly; a plot of $1/k_{\text{obs}}$ is linear in [L] (Figure 2.21). In principle, at sufficiently high [L] some **18** should form directly in competition with **17**; in practice, such conditions are probably not reachable (and conversion of **12** would become extremely slow anyway).

Figure 2.21. Dependence of the reciprocal of the rate of conversion of **12** to **17** on the amount of added triphenylphosphine. See Section 2.5.2 for details on how this plot was constructed.

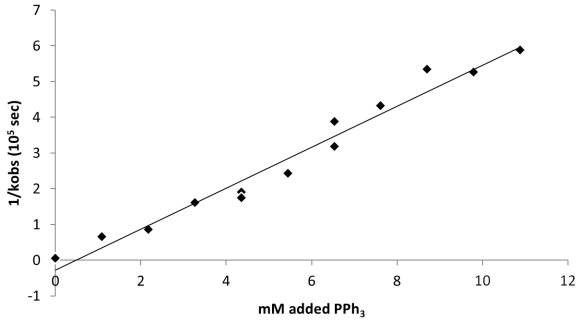

The rate law for direct conversion of **12** to **18** in *p*-xylene should be identical to the above, and the reaction does exhibit clean first-order kinetics, at a rate ($k_{\text{obs}} = 8(1) \times 10^{-5}$ s^{-1}) about a factor of 2 slower than that for **12** to **17**. There are several possible explanations for the discrepancy. First, the values of K_1 and k_2 need not be identical to those in benzene (though they would not be expected to differ very much). Second, intermediate **C** may be complexed by *p*-xylene to give

an analogue of intermediate **D**, which in this case (in contrast to benzene) would not lead to any productive reaction, but would reduce the concentration of **C** and hence the rate of formation of **18**. However, any substantial (i.e. sufficient to account for the entire factor of 2) concentration of a new intermediate should have been detectable by NMR. Finally (and perhaps most likely), it may be that agreement within a factor of 2 (especially on changing solvent) is as good as can be expected, given the reproducibility considerations discussed earlier.

As noted above, the conversion of **17** to **18** is much slower in benzene than in *p*-xylene, taking place over weeks or days, respectively (Figure 2.22). This observation is readily explained by Scheme 2.9: the concentration of **C**, the precursor to **18**, will be inversely related to the concentration of benzene. The rate law for that mechanism can be derived by using the steady-state approximation for *both* **C** and **F**, both of which should be present in low concentration and in rapid equilibrium with one another. This is most simply accomplished by defining a dummy variable $[\mathbf{X}] = [\mathbf{C}] + [\mathbf{F}]$. For steady-state in $[\mathbf{X}]$: $0 = d[\mathbf{X}]/dt = k_{-4}[\mathbf{17}] - k_4[\mathbf{F}][\mathrm{L}] - k_5[\mathbf{C}][\mathrm{L}]$. Substituting $[\mathbf{F}] = K_3[\mathbf{C}][\mathrm{PhH}]$ gives $k_{-4}[\mathbf{17}] - k_4[\mathbf{F}][\mathrm{L}] - k_5[\mathbf{C}][\mathrm{L}] = k_{-4}[\mathbf{17}] - K_3k_4[\mathbf{C}][\mathrm{PhH}][\mathrm{L}] - k_5[\mathbf{C}][\mathrm{L}] = 0$; hence $[\mathbf{C}] = (k_{-4}[\mathbf{17}])/(k_5[\mathrm{L}] + K_3k_4[\mathrm{PhH}][\mathrm{L}])$. Hence the rate law for the conversion is $-d[\mathbf{17}]/dt = d[\mathbf{18}]/dt = k_5[\mathbf{C}][\mathrm{L}] = (k_{-4}k_5[\mathbf{17}])/(k_5 + K_3k_4[\mathrm{PhH}])$. In benzene solution the reaction should be first-order in **17** and independent of [L]; both were observed. In *p*-xylene, on the other hand, [PhH] is continuously increasing as **17** is consumed, so first-order kinetics (which *are* observed) would not be expected *unless* k_5 is large compared to $k_4K_3[\mathrm{PhH}]$ over the course of the reaction.

Figure 2.22. Kinetics for conversion of **17** to **18** in C_6D_6 (left) and *p*-xylene-d_{10} (right) at 65°C.

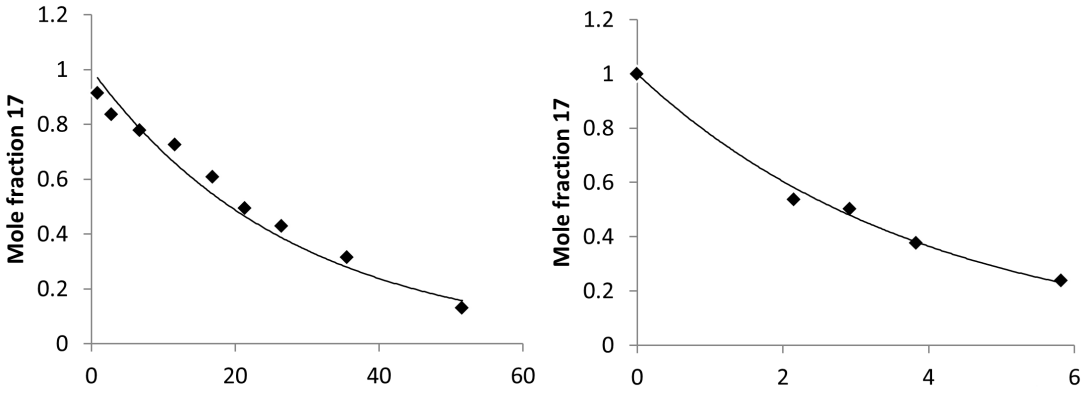

We can test this for self-consistency with the observed rate constants, again assuming that there is little difference in parameters between benzene and *p*-xylene reactions. For conversion of **17** to **18** in benzene, $k_{\mathrm{obs}} = 4.2(6) \times 10^{-7}\ \mathrm{s}^{-1}$. Since no direct formation of **18** from **12** was observed, k_5 must be small compared to $k_4K_3[\mathrm{PhH}]$, so that value of k_{obs} is approximately equal to $k_{-4}k_5/k_4K_3[\mathrm{PhH}]$. For the reaction in *p*-xylene, $k_{\mathrm{obs}} = 2.9(4) \times 10^{-6}\ \mathrm{s}^{-1}$; if our assumption that k_5 is large compared to $k_4K_3[\mathrm{PhH}]$ is correct, *that* value of $k_{\mathrm{obs}} = k_{-4}$. Substituting this value into

the above expression, we get k_5/k_4K_3[PhH] = 0.13, so k_5 is not completely negligible compared to k_4K_3[PhH], but small enough (within the limits of reproducibility as well as the assumption of solvent-independent parameters) to validate the approximation for k_{obs} in benzene. Furthermore, since for neat benzene [PhH] ≈ 11 M, k_5/k_4K_3 = 1.4 M. For the reaction in *p*-xylene, the starting [**17**] = the maximum [PhH] = 8.8 mM and the minimum value of k_5/k_4K_3[PhH] = 160, so the assumption required to account for first-order kinetics is valid as well. Accordingly, the kinetics appear completely consistent with the proposed mechanism.

2.4 Conclusions

The ONO ligand provides a versatile framework for synthesis of a wide variety of Ir^{I} and Ir^{III} complexes. Using this framework, two key steps in a scheme for functionalization of hydrocarbons have been demonstrated. Conversion of the Ir−Me bond in complexes **12** and **14** to MeI is effected by addition of I_2; there is evidence that the reaction proceeds *via* one-electron oxidation to an (isolable) Ir^{IV} methyl intermediate. Triphenylphosphine complex **12** is able to activate C−H bonds in benzene (and toluene) under quite mild conditions; the mechanism follows an unusual pathway in which the first C−H activation is intramolecular, but the product of that process, although thermodynamically preferred, is kinetically disfavored with respect to the intermolecular benzene activation product. Unfortunately the (ONO)Ir^{III} system is not sufficiently reactive to activate nonaromatic C−H bonds (except for acetonitrile).

2.5 Supporting Details

2.5.1 Experimental Section

2.5.1.1 General Methods

All compounds were prepared in a nitrogen-filled glovebox unless otherwise specified. Reactions taking place in dichloromethane at 90°C were conducted in either sealed glass bombs or J-Young NMR tubes. Solvents in the glovebox were dried using the Grubbs method [18]. All NMR solvents were purchased from Cambridge Isotope Laboratories, Inc., (except for $CDCl_3$) filtered through alumina, and stored over 4 Å molecular sieves. $POCl_3$ was purchased from Acros Organics. 2,6-dibromopyridine, *n*BuLi, *t*BuLi, 4-*tert*-butylpyridine, [$FeCp_2$][PF_6], indene, *N*,*N*-dimethylaminoethanol, PPh_3, propylene, proton sponge, $AgPF_6$, AgOTf, 15-crown-5, and NaH were purchased from Aldrich. H_2O_2 was purchased from EMD. [Ir(cod)Cl]$_2$ and Pd(PPh_3)$_4$ were purchased from Strem. The synthetic route towards the ligand H_2(ONO) closely follows a previously described procedure [9]. ^{1}H, ^{13}C, ^{19}F, and ^{31}P NMR spectra were recorded on Varian Mercury 300 MHz NMR spectrometers. X-ray data were

collected using a Bruker KAPPA APEX II diffractometer.

2.5.1.2 Synthesis of 4-*tert*-Butylpyridine-*N*-oxide

Following a published procedure [19], 4-*tert*-butylpyridine (18.0 mL, 16.6 g, 123 mmol) was mixed with 135 mL of glacial acetic acid and 100 mL of hydrogen peroxide (30% in water) in a 1 L round-bottom flask under air. After refluxing for 4 h, 100 mL of additional hydrogen peroxide (30% in water) was added, and the mixture was refluxed overnight. Then 200 mL of the solvent was removed by distillation, and 100 mL water was added and then removed by distillation as well. The remaining solution was neutralized with sodium carbonate. The organic layer was extracted with methylene chloride, filtered, and evaporated to dryness to yield white crystals (which gave a yellow solution in CH_2Cl_2). Isolated yield: 15.3 g, 101 mmol, 82%. ^{1}H NMR (300 MHz, $CDCl_3$): δ 1.31 (s, 9H, $C(CH_3)_3$), 7.26 (d, 2H, ^3J = 7.2 Hz, aryl-H), 8.15 (d, 2H, ^3J = 7.5 Hz, aryl-H). ^{13}C{^{1}H} NMR (75.4 MHz, $CDCl_3$): δ 30.5 ($C(CH_3)_3$), 34.6 ($C(CH_3)_3$), 123.1, 138.6, 151.2 (aryl).

2.5.1.3 Synthesis of 2-Chloro-4-*tert*-butylpyridine

In a 250 mL round-bottom flask open to the air, 4-*tert*-butylpyridine-*N*-oxide (15.3 g, 101 mmol) was dissolved in 61 mL of neat $POCl_3$. The mixture was allowed to reflux under argon for 12 to 16 h (refluxing can also be done under air, but the yield is somewhat lower). Excess $POCl_3$ was removed by distillation, and the remaining liquid was washed with a saturated aqueous solution of sodium carbonate. The organic layer was extracted with ether, filtered, and evaporated to dryness, yielding a dark red oil (13.5 g, 79.3 mmol, 79% yield). ^{1}H NMR (300 MHz, $CDCl_3$): δ 1.26 (s, 9H, $C(CH_3)_3$), 7.16 (dd, 1H, ^3J = 5.4 Hz, ^4J = 1.8 Hz, aryl-H), 7.25 (d, 1H, ^4J = 1.8 Hz, aryl-H), 8.23 (dd, 1H, ^3J = 5.7 Hz, ^5J = 0.6 Hz, aryl-H). ^{13}C{^{1}H} NMR (75.4 MHz, $CDCl_3$): δ 30.3 ($C(CH_3)_3$), 35.0 ($C(CH_3)_3$), 119.7, 121.3, 149.4, 151.7, 163.5 (aryl).

2.5.1.4 Synthesis of 2-Chloro-4-*tert*-butylpyridine-*N*-oxide

In a 1 L round-bottom flask, 2-chloro-4-*tert*-butylpyridine (13.5 g, 79.3 mmol) was mixed with 100 mL of glacial acetic acid and 80 mL of hydrogen peroxide (30% in water). After refluxing for 4 h under air, 80 mL of additional hydrogen peroxide (30% in water) was added and the mixture was refluxed overnight. Then 200 mL of the solvent was removed by distillation, and 100 mL of water was added and then distilled off as well. The remaining solution was neutralized with sodium carbonate. The organic layer was extracted with methylene chloride, filtered, and evaporated to dryness to yield yellow crystals (10.3 g, 55.3 mmol, 70% yield). ^{1}H NMR (300 MHz, $CDCl_3$): δ 1.31 (s, 9H, $C(CH_3)_3$), 7.19 (dd, 1H, ^3J = 6.6 Hz, ^4J = 3.0 Hz, aryl-H), 7.44 (d, 1H, ^4J = 2.7 Hz, aryl-H), 8.27 (dd, 1H, $^3J = 6.6Hz$, ^5J = 0.6 Hz, aryl-H). ^{13}C{^{1}H} NMR (75.4 MHz, $CDCl_3$): δ 30.4 ($C(CH_3)_3$), 34.7 ($C(CH_3)_3$), 121.3, 124.1, 139.8, 151.3 (aryl).

2.5.1.5 Synthesis of 2,6-Dichloro-4-*tert*-butylpyridine

In a 250 mL round-bottom flask open to the air, 2-chloro-4-*tert*-butylpyridine-*N*-oxide (15.3 g, 101 mmol) was dissolved in 40 mL of neat $POCl_3$. The mixture was allowed to reflux under argon for 12 to 16 h. Excess $POCl_3$ was removed by distillation, and the remaining liquid was washed with a saturated aqueous solution of sodium carbonate. The organic layer was extracted with ether, filtered, and evaporated to dryness, yielding a thick black oil. This oil was subjected to column chromatography over silica (95:5 hexanes/ethyl acetate), affording brown crystals after evaporation of solvent. The crystals were washed with hexanes, giving white 2,6-dichloro-4-*tert*-butylpyridine (5.57 g, 27.3 mmol, 49% yield; yield over four steps from 4-*tert*-butylpyridine: 22%). ^{1}H NMR (300 MHz, $CDCl_3$): δ 1.30 (s, 9H, $C(CH_3)_3$), 7.23 (s, 2H, aryl-H). $^{13}C\{^1H\}$ NMR (75.5 MHz, $CDCl_3$): δ 30.3 ($C(CH_3)_3$), 35.4 ($C(CH_3)_3$), 120.2, 150.6, 166.3 (aryl).

2.5.1.6 Synthesis of *O*-Methoxymethyl-2-bromo-4,6-di-*tert*-butylphenoxide

Bromine (3.7 mL, 12 g, 73 mmol) was added *via* syringe to a solution of 2,4-di-*tert*-butylphenol (15 g, 73 mmol) in CH_2Cl_2 (200 mL). The brown color of Br_2 disappeared upon addition. GC-MS analysis after 5 min shows only the presence of the desired brominated product(M^+ = 284 and 286). The organic mixture was washed with water, then dried over $MgSO_4$, and filtered. Removal of volatile material by rotary evaporation gave a golden oil which solidified after placing under high vacuum ($<$ 1 mTorr). This material (4,6-di-*tert*-butyl-2-bromophenol) was dissolved in dry THF (200 mL) under argon, and was deprotonated with NaH (1.92 g, 80 mmol). After the addition of NaH the reaction mixture was stirred for 1 h at room temperature; then MOMCl (6.1 mL, 6.5 g, 80 mmol) was added *via* syringe. The reaction mixture was stirred at room temperature for 9 h. Water was added and the mixture was concentrated under vacuum. The desired product was extracted with CH_2Cl_2 (three times); the combined organic fractions were dried over $MgSO_4$, filtered, and dried under high vacuum overnight to give 23.5 g (98% yield over two steps) of *O*-methoxymethyl-2-bromo-4,6-di-*tert*-butylphenoxide as a golden oil. ^{1}H NMR (300 MHz, $CDCl_3$): δ 1.30 (s, 9H, $C(CH_3)_3$), 1.44 (s, 9H, $C(CH_3)_3$), 3.70 (s, 3H, OCH_3), 5.23 (s, 2H, OCH_2O), 7.32 (d, 2H, aryl-H), 7.41 (d, 2H, aryl-H). $^{13}C\{^1H\}$ NMR (75.4 MHz, $CDCl_3$): δ 31.0 ($C(CH_3)_3$), 31.5 ($C(CH_3)_3$), 34.8 ($C(CH_3)_3$), 36.1 ($C(CH_3)_3$), 57.9 (OCH_3), 99.5 (OCH_2O), 117.7, 124.1, 128.9, 144.6, 147.8, 150.7 (aryl). MS FAB+: 328 (M^+).

2.5.1.7 Synthesis of $MOM_2(ONO)$

A mixture of *O*-Methoxymethyl-2-bromo-4,6-di-*tert*-butylphenoxide (5.19 g, 15.8 mmol) and THF (25 mL) in a Schlenk tube fitted with a screw-in Teflon stopper was frozen in a cold well, along with a solution of *t*BuLi (2.13 g, 33.3 mmol, 2.1 eq) in hexanes (10 mL), in an inert atmosphere

glove box. Both solutions were taken out of the box, and the *t*BuLi solution was added to the solution of *O*-Methoxymethyl-2-bromo-4,6-di-*tert*-butylphenoxide while allowing the latter to thaw. The mixture was stirred for 1 h while allowing it to reach room temperature. $ZnCl_2$ (1.51 g, 7.12 mmol, 0.70 eq) was added with the aid of THF. After stirring the reaction mixture for 30 minutes, 1,3-dibromobenzene (1.69 g, 7.12 mmol, 0.45 eq) and $Pd(PPh_3)_4$ (188.4 mg, 0.163 mmol, 0.01 eq) were added with the aid of some THF. The reaction vessel was placed in an oil bath preheated to 75°C and stirred for 16 h, then allowed to cool to room temperature and quenched with water. Volatile materials were removed under vacuum and water was added. This mixture was extracted with Et_2O (three times). The combined organics were dried over $MgSO_4$, filtered, and concentrated by rotary evaporation. The resulting residue was suspended in MeOH cooled to −25°C. The resulting white precipitate was collected by filtration through a sintered glass funnel, washed with cold MeOH, and immediately used for the synthesis of H_2(ONO). ^{1}H NMR (300 MHz, $CDCl_3$): δ 1.37 (s, 18H, $C(CH_3)_3$), 1.51 (s, 18H, $C(CH_3)_3$), 3.41 (s, 6H, OCH_3), 4.64 (s, 4H, OCH_2O), 7.45 (d, 2H, aryl-H), 7.61 (d, 2H, aryl-H), 7.68 − 7.80 (m, 3H, NC_5H_3). $^{13}C\{^1H\}$ NMR (75.4 MHz, $CDCl_3$): δ 31.1 ($C(CH_3)_3$), 31.6 ($C(CH_3)_3$), 34.8 ($C(CH_3)_3$), 35.6 ($C(CH_3)_3$), 57.6 (OCH_3), 99.7 (OCH_2O), 123.2, 125.2, 126.7, 134.1, 136.1, 142.5, 146.1, 151.5, 158.4 (aryl).

Synthesis of H_2(ONO)

Compound MOM_2(ONO) was suspended in 25 mL of MeOH, and 25 mL of concentrated HCl was added. This mixture was heated at 80°C for 5 h. After cooling, volatile materials were removed under vacuum yielding 3.45 g (0.70 mmol, 90% based on *O*-Methoxymethyl-2-bromo-4,6-di-*tert*-butylphenoxide) of H_2(ONO) as a white powder. ^{1}H NMR (300 MHz, $CDCl_3$): δ 1.39 (s, 18H, $C(CH_3)_3$), 1.48 (s, 18H, $C(CH_3)_3$), 7.46 (d, 2H, aryl-H), 7.51 (d, 2H, aryl-H), 7.67 (d, 2H, 3_5−NC_5H−H_2), 8.01 (t, 1H, 4-NC_5H_2−H), 10.59 (s, 2H, OH). $^{13}C\{^1H\}$ NMR (75.4 MHz, $CDCl_3$): δ 29.8 ($C(CH_3)_3$), 31.8 ($C(CH_3)_3$), 34.6 ($C(CH_3)_3$), 35.6 ($C(CH_3)_3$), 120.5, 121.3, 123.0, 126.4, 137.5, 140.0, 141.5, 153.3, 157.6 (aryl). HR-MS: $C_{33}H_{45}O_2N$: Calculated: 487.3450. Measured: 487.3446.

2.5.1.8 Synthesis of $MOM_2(ONO^{tBu})$

O-Methoxymethyl-2-bromo-4,6-di-*tert*-butylphenoxide (6.15 g, 18.7 mmol), was dissolved in 60 mL of THF. *tert*-butyllithium (2.52 g, 39.4 mmol) was dissolved in 27 mL of pentane and added to the solution of *O*-methoxymethyl-2-bromo-4,6-di-*tert*-butylphenoxide at −78°C. The mixture was allowed to warm to room temperature and stirred for 1 h. A suspension of $ZnCl_2$ (1.80 g, 13.2 mmol) in THF was then added, and the mixture stirred for another 30 min. A solution of 2,6-dichloro-4-*tert*-butylpyridine (1.72 g, 8.42 mmol) and $Pd(PPh_3)_4$ (218 mg, 189 μmol) in THF was added, the reaction vessel was transferred to a preheated 75°C oil bath, and the mixture was stirred for 16 h. The

mixture was quenched with 10 mL of water, and the volatiles were removed by rotary evaporation. Another 70 mL of water was then added, and the organic layer was extracted three times with ether, dried with $MgSO_4$, and evaporated to dryness, giving a white powder, which was purified by washing with cold methanol (2.67 g, 4.23 mmol, 50.3% yield). ^{1}H NMR (300 MHz, $CDCl_3$): δ 1.35 (s, 18H, $C(CH_3)_3$), 1.37 (s, 9H, $C(CH_3)_3$), 1.49 (s, 18H, $C(CH_3)_3$), 3.38 (s, 6H, OCH_3) 4.60 (s, 4H, OCH_2O), 7.42 (d, 2H, ^4J = 2.6 Hz, aryl-H), 7.56 (d, 2H, ^4J = 2.6 Hz, aryl-H), 7.66 (s, 2H, NC_5H_2). $^{13}C\{^1H\}$ NMR (75.4 MHz, $CDCl_3$): δ 30.6, 30.9, 31.4, 34.6, 34.9, 35.4 ($C(CH_3)_3$), 57.3 (OCH_3), 99.3 (OCH_2O), 120.4, 124.8, 126.6, 134.3, 142.2, 145.8, 151.3, 158.0, 159.7 (aryl).

2.5.1.9 Synthesis of $H_2(ONO^{tBu})$

$MOM_2(ONO^{tBu})$ (2.67 g, 4.23 mmol) was suspended in a mixture of methanol (40 mL) and concentrated HCl (40 mL) and heated at 80°C for 6 h. The suspension was then cooled to 0°C and filtered, and the precipitate, a white powder, was washed with cold MeOH to afford $H_2(ONO^{tBu})$ (1.71 g, 3.14 mmol, 74% yield). ^{1}H NMR (300 MHz, d_8-THF): δ 1.36 (s, 18H, $C(CH_3)_3$), 1.46 (br, 27H, $C(CH_3)_3$), 7.42 (d, 2H, ^4J = 2.4 Hz, aryl-H), 7.53 (d, 2H, ^4J = 2.7 Hz, aryl-H), 7.81 (s, 2H, NC_5H_2), 10 (br s, concentration dependent, 2H, OH). $^{13}C\{^1H\}$ NMR (75.4 MHz, $CDCl_3$): δ 29.6, 30.6, 31.6, 34.4, 35.3, 35.5 ($C(CH_3)_3$), 117.7, 121.7, 122.6, 126.0, 137.2, 141.2, 153.0, 157.2, 164.1 (aryl). MS FAB+: 543.4052 (M^+). Analysis calculated for $C_{37}H_{53}NO_2$: C, 81.72; H, 9.82; N, 2.58. Found: C, 81.57; H, 10.06; N, 2.55.

2.5.1.10 Synthesis of Na[Ir(cod)ONO], 1

$H_2(ONO)$ (91.2 mg, 187 μmol) was dissolved in 10 mL of THF, and an excess of NaH (24.6 mg, 1.03 mmol) was added. The yellow suspension first turned orange and then yellow again, with vigorous evolution of H_2. The suspension was allowed to stir for one hour, after which it was filtered through Celite and added to a stirring solution of $[Ir(cod)Cl]_2$ (60.0 mg, 89.3 μmol) in 5 mL of THF. After 30 min of stirring the solution was filtered and pumped down, giving **1** as a red powder. Residual solvent was removed by trituration with benzene followed by overnight evacuation under high vacuum. Isolated yield was 148.3 mg (183.3 μmol, 98.0%); the yield was quantitative by NMR. ^{1}H NMR (300 MHz, d_8-THF): δ 0.84 (m, 4H, sp^3 on cod), 1.32 (s, 18H, 2 *t*Bu on ligand phenolate), 1.49 (s, 18H, 2 *t*Bu on ligand phenolate), 1.68 (br m, 4H, sp^3 on cod), 2.99 (br d, 4H, J = 2.7 Hz, sp^2 on cod), 7.19 (d, 2H, ^4J = 2.7 Hz, ligand aryl), 7.24 (d, 2H, ^4J = 2.6 Hz, ligand aryl), 7.26 (br s, 2H, ligand aryl), 7.66 (t, 1H, ^3J = 8.0 Hz, ligand pyridine 4-position). $^{13}C\{^1H\}$ NMR (75.4 MHz, d_8-THF): δ 14.6, 23.4, 31.5, 32.5, 32.8, 34.7, 36.2, 49.7, 121.3, 123.8, 125.0, 131.9, 135.7, 137.2, 139.2, 159.4, 166.9. MS FAB+: 786.3856 (M^+−Na).

2.5.1.11 Synthesis of Pyridine-Activated Complex 3

Na[Ir(cod)(ONO)] (**1**) (85.1 mg, 105 μmol) was dissolved in 1 mL of C_6H_6. 15-Crown-5 (21 μL, 106 μmol) was mixed in, and the solution was allowed to sit undisturbed for several days. Orange crystals formed and were shown crystallographically to consist of **3**. A pure (by NMR) sample was obtained by washing with C_6H_6, redissolving in THF, and drying under vacuum. Isolated yield: 82.7 mg (79.8 μmol, 75.9%). ^{1}H NMR (500 MHz, d_8-THF): δ 1.35 (s, 9H, *t*Bu on ligand phenolate), 1.42 (s, 9H, *t*Bu on ligand phenolate), 1.51 (br s, 18H, 2 *t*Bu on ligand phenolate), 1.77 (br, 4H, sp^3 on cod), 2.18 (br, 4H, sp^3 on cod), 3.29 (br, 2H, sp^2 on cod), 3.37 (s, 20H, crown ether), 4.46 (br, 2H, sp^2 on cod), 7.24 (d, 1H, ^4J = 2.6 Hz, ligand aryl), 7.25 (d, 1H, ^4J = 2.4 Hz, ligand aryl), 7.48 (d, 1H, ^3J = 8.4 Hz, ligand aryl), 7.78 (d, 1H, ^4J = 2.4 Hz, ligand aryl), 7.91 (d, 1H, ^3J = 8.2 Hz, ligand aryl), 8.45 (d, 1H, ^4J = 2.6 Hz, ligand aryl), 18.14 (s, 1H, ligand phenol). ^{13}C{^{1}H} NMR (126 MHz, d_8-THF): δ 30.4, 31.1, 31.6, 32.4, 32.9, 33.9, 35.1, 35.4, 36.1, 36.4, 45.1, 70.2, 74.4, 112.5, 120.2, 120.8, 123.0, 124.3, 124.4, 126.9, 135.0, 137.4, 138.5, 138.8, 146.5, 149.7, 152.6, 153.2, 159.7, 162.7.

2.5.1.12 Synthesis of [NaIr(cod)(ONO$^{t\mathrm{Bu}}$)]$_2$, 4

H_2(ONO$^{t\mathrm{Bu}}$) (246.8 mg, 453.8 μmol) was dissolved in 10 mL of THF, and an excess of NaH (64.8 mg, 2.70 mmol) was added. The light yellow solution first turned orange and then yellow again, with vigorous evolution of H_2. The suspension was allowed to stir for an hour, after which it was filtered through Celite. [Ir(cod)Cl]$_2$ (145.2 mg, 216.2 μmol) was dissolved in THF and slowly added to the stirring solution of Na_2(ONO$^{t\mathrm{Bu}}$) in order to prevent formation of overmetalated [Ir(cod)]$_2$(ONO$^{t\mathrm{Bu}}$), **5**. After an hour of stirring the solvent was removed *in vacuo*, redissolved in hexanes, and filtered, and the solvent removed *in vacuo* again, giving **4**·THF as a red solid with a glassy appearance. The residual THF was removed by adding more hexanes and evacuating to give **4**. **4**·THF is very soluble in hexanes, whereas **4** is much less so; consequently impurities in **4** can be removed with a hexanes wash. Crystals were obtained by allowing a pentane solution of **4**·THF or **4** to evaporate. Isolated yield was 326.4 mg (188.6 μmol, 87.2%). ^{1}H NMR (300 MHz, d_8-THF): δ 0.83 (br d, 16H, ^2J = 7.5 Hz, sp^3 on 2 cod), 1.33 (s, 36H, 4 *t*Bu on ligand phenolate), 1.37 (s, 18H, 2 *t*Bu on ligand pyridine), 1.49 (s, 36H, 4 *t*Bu on ligand phenolate), 2.97 (br s, 8H, sp^2 on 2 cod), 7.19 (d, 4H, ^4J = 2.7 Hz, 2 ligand phenolate aryl), 7.23 (d, 4H, ^4J = 3.0 Hz, 2 ligand phenolate aryl), 7.25 (s, 4H, 2 ligand pyridine aryl). ^{13}C{^{1}H} NMR (75.4 MHz, d_8-THF): δ 31.6, 32.1, 33.1, 33.5, 35.4, 36.2, 36.9, 50.3, 119.2, 124.4, 125.4, 133.0, 136.2, 139.6, 159.6, 161.2, 167.7. MS FAB+: 842.4478 ([Ir(cod)(ONO$^{t\mathrm{Bu}}$) (M$^+$−Na). Analysis calculated for $C_{90}H_{126}Ir_2N_2Na_2O_4$: C, 62.47; H, 7.34; N, 1.62. Found: C, 62.26; H, 7.52; N, 1.35.

2.5.1.13 Reaction of 4 with CO

$[NaIr(cod)(ONO^{tBu})]_2$ (179.4 mg, 103.7 μmol) was dissolved in THF in a Schlenk flask. The solution was cooled to $-78°C$, and an atmosphere of CO (about 5 mmol) was introduced into the headspace. The solution was then brought back to room temperature and allowed to stir overnight. Afterward, the solution was pumped down, yielding a yellow-brown solid with IR stretching frequencies at 2057, 2030, and 1977 cm^{-1}. This solid was reintroduced into the glovebox, redissolved in pentane, and filtered. Allowing the pentane solution to slowly evaporate yielded brown crystals. X-ray diffraction of the crystals revealed their identity to be $Ir_4(CO)_{12}$, consistent with the aforementioned IR stretching frequencies.

2.5.1.14 Reaction of 4 with H_2

$[NaIr(cod)(ONO^{tBu})]_2$ (10.2 mg, 5.89 μmol) was dissolved in 0.7 mL of d_8-THF in a J-Young NMR tube. Two drops of benzene were added as an internal standard. The headspace was then charged with 2.9 atm H_2, and the NMR tube continuously inverted for mixing. After 11 h, the solution color had lightened considerably, and an iridium mirror had deposited. ^{1}H NMR showed quantitative conversion to the protonated ligand $H_2(ONO^{tBu})$.

2.5.1.15 Synthesis of $[Ir(cod)]_2(ONO^{tBu})$, 5

$H_2(ONO^{tBu})$ (57.6 mg, 106 μmol) was dissolved in 5 mL of THF, and an excess of NaH (30.2 mg, 1.26 mmol) was added. The yellow suspension first turned orange and then yellow again, with vigorous evolution of H_2. The suspension was allowed to stir for an hour, after which it was filtered through Celite. A 5 mL THF solution of $[Ir(cod)Cl]_2$ (71.1 mg, 107 μmol) was then added while stirring. After 1 h of stirring, the solvent was removed *in vacuo*; and the orange compound was redissolved in pentane and filtered. The solvent was then removed *in vacuo* again, giving **5** as an orange powder. Crystals were obtained by allowing a pentane solution to evaporate. Yield was 119.3 mg (104 μmol, 98.6%). ^{1}H NMR (300 MHz, d_8-THF): δ 0.81 (br d, 16H, $^2J = 6.9$ Hz, sp^3 on 2 cod), 1.39 (s, 18H, 2 *t*Bu on ligand phenolate), 1.52 (s, 9H, *t*Bu on ligand pyridine), 1.58 (s, 18H, 2 *t*Bu on ligand phenolate), 3.08 (br s, 8H, sp^2 on 2 cod), 7.51 (br d, 4H, $J = 5.4$ Hz, 2 ligand phenolate aryl), 7.82 (s, 2H, ligand pyridine aryl). $^{13}C\{^1H\}$ NMR (75.4 MHz, d_8-THF): 15.2, 24.1, 31.0, 31.6, 32.65, 32.75, 33.4, 35.1, 35.8, 35.9, 36.9, 38.3, 56.1, 121.7, 124.9, 130.0, 134.9, 139.2, 141.8, 159.3, 163.1, 163.6. MS FAB+: 1141.5018 (M^+ with ^{191}Ir), 843.4935 ($[Ir(cod)(ONO^{tBu})]^+$). Analysis calculated for $C_{53}H_{75}Ir_2NO_2$: C, 55.71; H, 6.62; N, 1.23. Found: C, 54.81; H, 6.77; N, 1.12.

Alternatively, $[NaIr(cod)(ONO^{tBu})]_2$ (15 mg, 9 μmol) was dissolved in 1 mL of THF. $[Ir(cod)Cl]_2$ (6 mg, 9 μmol) was dissolved in 2 mL of THF and added. After two hours the solution was the solvent was removed *in vacuo*, redissolved in pentane, and filtered, and the solvent removed *in vacuo* again,

giving 5 (20 mg, 18 μmol, 100% yield) as an orange powder. Characterization data were as reported above.

2.5.1.16 Synthesis of [(ONO$^{t\mathrm{Bu}}$)Ir(cod)(MeCN)][PF$_6$], 6

[NaIr(cod)(ONO$^{t\mathrm{Bu}}$)]$_2$ (106.3 mg, 61.4 μmol) was dissolved in 10 mL of THF. A solution of $AgPF_6$ (59.4 mg, 235 μmol) in acetonitrile was added, resulting in the mixture immediately turning black. The solution was allowed to stir overnight. Afterward, the solvent was removed *in vacuo*, and the black solid redissolved in benzene, filtered, and lyophilized to give **6** as a yellow powder. This complex was recrystallized by layering pentane onto a benzene solution. Yield after recrystallization was 93.0 mg (90.4 μmol, 73.6%). ^{1}H NMR (300 MHz, CD_3CN): δ 1.37 (s, 18H, 2 *t*Bu on ligand phenolate), 1.45 (s, 9H, *t*Bu on ligand pyridine), 1.53 (s, 18H, 2 *t*Bu on ligand phenolate), 2.26 (m, 4H, sp^3 on cod), 2.42 (s, 3H, MeCN ligand), 2.75 (br s, 2H, sp^3 on cod), 4.31 (br s, 2H, sp^3 on cod), 5.45 (m, 2H, sp^2 on cod), 6.65 (m, 2H, sp^2 on cod), 7.41 (two overlapping peaks, s, 4H, 2 ligand phenolate aryl), 7.70 (s, 2H, ligand pyridine aryl). ^{13}C{^{1}H} NMR (75.4 MHz, C_6D_6): δ 1.3, 28.0, 29.3, 29.4, 30.3, 31.2, 33.9, 34.4, 35.5, 100.2, 113.9, 119.9, 120.6, 123.2, 125.8, 126.4, 139.4, 140.7, 154.3, 161.8, 162.1. ^{19}F{^{13}C} NMR (282 MHz, C_6D_6): δ -71.1 (d, $^1J_{\mathrm{PF}} = 711$ Hz). ^{31}P{^{1}H} NMR (122 MHz, C_6D_6): δ -143.2 (septet, $^1J_{\mathrm{PF}} = 711$ Hz). MS FAB+: 842.4472 ([Ir(cod)(ONO$^{t\mathrm{Bu}}$)]$^+$). Analysis calculated for $C_{47}H_{66}F_6IrN_2O_2P \cdot C_6H_6$: C, 57.54; H, 6.56; N, 2.53. Found: C, 57.06; H, 6.48; N, 2.42.

Alternatively, [NaIr(cod)(ONO$^{t\mathrm{Bu}}$)]$_2$ (103.9 mg, 60.0 μmol) was dissolved in 10 mL of THF. A suspension of [$FeCp_2$][PF_6] (75.6 mg, 228 μmol) in acetonitrile was added, the solution was allowed to stir overnight, the solvent was removed *in vacuo*, and the solid redissolved in benzene, filtered, and lyophilized to give **6**. Yield after recrystallization (as above) was 98.7 mg (96.0 μmol, 79.9%). Characterization data were as reported above.

2.5.1.17 Synthesis of (ONO$^{t\mathrm{Bu}}$)Ir(cod)OTf, 7

[NaIr(cod)(ONO$^{t\mathrm{Bu}}$)]$_2$ (310.0 mg, 179.1 μmol) and AgOTf (175.7 mg, 683.8 μmol) were each dissolved in about 10 mL of benzene. The AgOTf solution was then added dropwise to the stirring solution of **4**. The mixture immediately turned black and was allowed to stir overnight. It was then filtered, pumped down, and washed with pentane, yielding (ONO$^{t\mathrm{Bu}}$)Ir(cod)OTf, **7** (259 mg, 261 μmol, 76% yield). Since **7** has limited solubility in benzene (about 10 mg/mL), it can be purified by washing with benzene. Crystals were obtained by layering a saturated benzene solution with pentane. ^{1}H NMR (300 MHz, C_6D_6): δ 0.93 (s, 9H, *t*Bu on ligand pyridine), 1.19 (br s, 8H, sp^3 on cod), 1.42 (s, 18H, 2 *t*Bu on ligand phenolate), 1.74 (s, 18H, 2 *t*Bu on ligand phenolate), 2.42 (br s, 2H, sp^2 on cod), 4.62 (m, 2H, sp^2 on cod), 7.35 (s, 2H, ligand pyridine aryl), 7.45 (d, 2H, $^4J = 2.7$ Hz, ligand phenolate aryl), 7.58 (d, 2H, $^4J = 2.7$ Hz, ligand phenolate aryl). ^{13}C{^{1}H} NMR (75.4 MHz, C_6D_6): δ 27.4, 29.5, 30.0, 30.7, 31.4, 34.0, 34.2, 35.7, 90.7, 112.8, 120.6, 123.3, 125.9, 126.2,

139.1, 139.6, 153.2, 160.9, 161.2. $^{19}F\{^{13}C\}$ NMR (282 MHz, C_6D_6): δ −77.6. MS FAB+: 991.5552 (M^+), 858.5524 ([(ONO^{tBu})Ir(cod)]$^+$). Analysis calculated for $C_{46}H_{63}F_3IrNO_5PS$: C, 55.74; H, 6.41; N, 1.41. Found: C, 55.51; H, 6.36; N, 1.38.

2.5.1.18 Synthesis of (ONO^{tBu})Ir(PPh$_3$)$_2$OTf, 8

7 (89.4 mg, 90.2 μmol) and PPh_3 (47.3 mg, 180 μmol) were each dissolved in benzene and mixed together. The mixture was stirred at 90°C for at least 3 h, filtered, and then lyophilized. **8** (117.6 mg, 83.5 μmol, 92.6% yield) was formed as a yellow powder, soluble in benzene and slightly soluble in pentane (about 1 mg/mL). **8** is stable for several days at 90°C with little decomposition. ^1H NMR (300 MHz, C_6D_6): δ 0.94 (s, 9H, *t*Bu on ligand pyridine), 1.25 (s, 18H, 2 *t*Bu on ligand phenolate), 1.35 (s, 18H, 2 *t*Bu on ligand phenolate), 6.52 (s, 2H, ligand pyridine aryl), 6.68 (d, 2H, ^4J = 2.4 Hz, ligand phenolate aryl), 6.87 (br s, 12H, triphenylphosphines), 7.16 (br s, 6H, triphenylphosphines), 7.18 (d, 2H, ^4J = 2.5 Hz, ligand phenolate aryl), 7.63 (br s, 12H, triphenylphosphines). $^{13}C\{^1H\}$ NMR (75.4 MHz, C_6D_6): δ 29.6, 29.7, 29.9, 31.2, 33.6, 35.7, 119.4, 123.2, 125.0, 125.6, 126−128 (may be obscured by C_6D_6), 129.6, 134.0, 135.1 (br), 136.7, 140.7, 141.1. $^{19}F\{^{13}C\}$ NMR (282 MHz, C_6D_6): δ −76.4. $^{31}P\{^1H\}$ NMR (122 MHz, C_6D_6): δ −17.2. MS FAB+: 1258.5423 ([Ir(PPh$_3$)$_2$(ONO^{tBu})]$^+$), 1145.3984 ([Ir(PPh$_3$)(ONO^{tBu})(OTf)]$^+$), 996.4537 ([Ir(PPh$_3$)(ONO^{tBu})]$^+$). Analysis calculated for $C_{74}H_{81}F_3IrNO_5P_2S$: C, 63.14; H, 5.80; N, 1.00. Found: C, 63.24; H, 5.95; N, 0.87.

2.5.1.19 Synthesis of (ONO^{tBu})Ir(PPh$_3$)$_2$OH, 9

8 (20.8 mg, 14.7 μmol) was dissolved in benzene, and 2 μL of H_2O was added *via* a microliter syringe. The mixture was stirred for one hour, after which proton sponge (3.6 mg, 17 μmol) dissolved in benzene was added. A precipitate was immediately observed, and the mixture was stirred for four hours, pumped down, redissolved in benzene, filtered, and lyophilized, giving **9** (18.8 mg, 14.7 μmol, quantitative yield) as a yellow powder. **9** is slightly soluble in pentane (about 3 mg/mL) and was crystallized by letting a pentane solution evaporate. ^1H NMR (300 MHz, C_6D_6): δ −1.63 (s, ^1H, IrOH), 1.05 (br, 27H, 2 *t*Bu on ligand phenolate, *t*Bu on ligand pyridine), 1.34 (s, 18H, 2 *t*Bu on ligand phenolate), 6.75 (br, 4H, 2 ligand phenolate aryl), 6.8 − 7.2 (many broad overlapping peaks, 30H, triphenylphosphines), 7.38 (br s, 2H, ligand pyridine aryl). $^{31}P\{^1H\}$ NMR (122 MHz, C_6D_6): δ −23.2. MS FAB+: 1275.5450 ([Ir(PPh$_3$)$_2$(ONO^{tBu})OH]$^+$), 1258.5423 ([Ir(PPh$_3$)$_2$(ONO^{tBu})]$^+$), 1013.4492 ([Ir(PPh$_3$)(ONO^{tBu})OH]$^+$). Analysis calculated for $C_{73}H_{82}IrNO_3P_2$: C, 68.73; H, 6.48; N, 1.10. Found: C, 68.71; H, 6.66; N, 1.10.

2.5.1.20 Synthesis of (ONO^{tBu})Ir(PPh$_3$)$_2$Cl, 10

8 (39.0 mg, 27.7 μmol) was dissolved in 3 mL of dichloromethane and heated to 90°C for five hours. The solution was then pumped down, redissolved in benzene, filtered, and lyophilized, giving **10** (35.4

mg, 27.4 μmol, 98.7% yield) as a yellow powder. ^{1}H NMR (300 MHz, CD_2Cl_2): δ 0.79 (s, 18H, 2 tBu on ligand phenolate), 1.12 (s, 9H, tBu on ligand pyridine), 1.27 (s, 18H, 2 tBu on ligand phenolate), 6.50 (d, 2H, $^{4}J = 2.5$ Hz, ligand phenolate aryl), 6.65 (s, 2H, ligand pyridine aryl), 6.93 (d, 2H, $^{4}J = 2.5$ Hz, ligand phenolate aryl), $6.9 - 7.3$ (many broad overlapping peaks, 30H, triphenylphosphines). ^{13}C{^{1}H} NMR (126 MHz, CD_2Cl_2): δ 29.6, 30.4, 31.9, 34.3, 34.9, 35.7, 120.2, 124.5, 125.1, 126.1, 127.4 (br), 127.8 (br), 128.3 (br), 129.7 (br), 133.7 (br), 136.3 (br), 136.8, 141.0, 155.7, 159.1, 170.1. ^{31}P{^{1}H} NMR (121 MHz, CD_2Cl_2): δ −25.1. MS FAB+: 1294.5082 ([Ir(PPh_3)$_2$(ONO$^{t\mathrm{Bu}}$)Cl]$^+$), 1257.5300 ([Ir(PPh_3)$_2$(ONO$^{t\mathrm{Bu}}$)]$^+$), 1031.3262 ([Ir(PPh_3)(ONO$^{t\mathrm{Bu}}$)Cl]$^+$). Analysis calculated for $C_{73}H_{81}ClIrNO_2P_2$: C, 67.75; H, 6.31; N, 1.08. Found: C, 68.60; H, 6.84; N, 1.07.

2.5.1.21 Synthesis of (ONO$^{t\mathrm{Bu}}$)Ir(PPh_3)$_2$H, 11

LiOMe (3.9 mg, 0.10 mmol) was dissolved in methanol, and **8** (67.2 mg, 47.7 μmol) was added while stirring. A light yellow filtrate formed overnight and was filtered out. When benzene was added to this filtrate, a black precipitate immediately formed, which was also filtered out. The remaining yellow solution was lyophilized, giving (ONO$^{t\mathrm{Bu}}$)Ir(PPh_3)$_2$H, **11** (37.6 mg, 29.9 μmol, 62.5% yield), as a yellow powder. ^{1}H NMR (300 MHz, C_6D_6): δ −15.4 (t, 1H, $^{2}J_{\mathrm{PH}} = 17.8$ Hz, IrH), 0.79 (s, 18H, 2 tBu on ligand phenolate), 1.17 (s, 9H, tBu on ligand pyridine), 1.41 (s, 18H, 2 tBu on ligand phenolate), $6.8 - 7.4$ (many broad overlapping peaks, 36H, ligand aryl, triphenylphosphine aryl). ^{13}C{^{1}H} NMR (75.4 MHz, C_6D_6): δ 28.4, 30.0, 31.7, 33.7, 34.2, 34.9, 118.6, 123.5, 124.9, 126-128 (may be obscured by C_6D_6), 128.9 (br), 134.3 (br), 135.2, 154.1, 158.0, 170.3. ^{31}P{^{1}H} NMR (122 MHz, C_6D_6): δ 9.8. MS FAB+: 1260.5502 ([Ir(PPh_3)$_2$(ONO$^{t\mathrm{Bu}}$)H$_2$]$^+$), 997.4542 ([Ir(PPh_3)(ONO$^{t\mathrm{Bu}}$)H]$^+$).

11 was also obtained from the following reactions, although in most cases it was observed only by NMR and could not be isolated cleanly:

- **8** (25.7 mg, 18.3 μmol) and proton sponge (3.8 mg, 17.7 μmol) were dissolved in benzene and mixed. The solution was heated to 90°C for 24 h. It was then pumped down, redissolved in pentane, filtered, and pumped down again. The yield of **11** was nearly quantitative (by NMR).

- **8** (11.3 mg, 7.2 μmol) and dihydroanthracene (1.3 mg, 7.2 μmol) were dissolved in C_6D_6 and mixed. $CoCp_2$ (1.4 mg, 7.4 μmol) dissolved in C_6D_6 was then added, and the entire mixture transferred to a J-Young NMR tube. After stirring for one hour, NMR revealed the formation of **11** as the major product.

- **8** (16.7 mg, 10.7 μmol) was dissolved in approximately 1 mL of C_6D_6 in a J-Young NMR tube, and an excess of solid NaH (30 mg, 1 mmol) was added. The NMR tube was heated to 90°C, and the reaction was followed by NMR; after 26 h the reaction was complete. The solution was then removed, filtered, and pumped down. Isolated yield was 11.8 mg, 9.4 μmol, 88%.

- **8** (38.4 mg, 27.3 μmol) was dissolved in approximately 5 mL of benzene, and $ZnEt_2$ (1.5 μL, 14 μmol) was added *via* a microliter syringe. The stirring solution first turned red and then yellow and was allowed to stir overnight. The solution was then pumped down, redissolved in pentane, filtered, and pumped down again to form **11** as a clean solid.

2.5.1.22 Synthesis of $(ONO^{tBu})Ir(PPh_3)_2Me$, 12

8 (203.8 mg, 144.8 μmol) was dissolved in benzene, and $ZnMe_2$ (6.2 μL, 90 μmol) was added *via* a microliter syringe. The solution was stirred at room temperature overnight, filtered, and then lyophilized. **12** (182.6 mg, 143.4 μmol, 99.0% yield) was formed as a yellow powder, soluble in benzene and slightly soluble in pentane, and could be recrystallized by layering pentane on a benzene solution. ^{1}H NMR (300 MHz, C_6D_6): δ 1.13 (s, 9H, *t*Bu on ligand pyridine), 1.18 (s, 18H, 2 *t*Bu on ligand phenolate), 1.40 (s, 18H, 2 *t*Bu on ligand phenolate), 3.03 (t, 3H, $^3J_{PH} = 6.1$ Hz, IrMe), 6.82 (d, 2H, $^4J = 2.4$ Hz, ligand phenolate aryl), 6.89 (br s, 12H, triphenylphosphines), 6.92 (s, 2H, ligand pyridine aryl), 7.19 (d, 2H, $^4J = 2.6$ Hz, ligand phenolate aryl), 7.16 (br s, 6H, triphenylphosphines), 7.46 (br s, 12H, triphenylphosphines). $^{13}C\{^1H\}$ NMR (75.4 MHz, CD_2Cl_2): δ −31.4 (t, $^2J_{PC} = 8.6$ Hz), 29.3, 29.9, 31.3, 33.6, 34.3, 35.1, 119.4, 123.3, 125.9, 126.1, 127.1, 128.7, 134.7 (br), 135.1, 140.3, 153.9, 157.8, 170.4. $^{31}P\{^1H\}$ NMR (122 MHz, C_6D_6): δ −14.6. MS FAB+: 1273.4640 (M^+), 1011.4714 ($[Ir(PPh_3)(ONO^{tBu})(Me)]^+$), 995.3394 ($[Ir(PPh_3)(ONO^{tBu})]^+$). Analysis calculated for $C_{74}H_{84}IrNO_2P_2$: C, 69.78; H, 6.65; N, 1.10. Found: C, 69.81; H, 6.53; N, 1.05.

2.5.1.23 Synthesis of $(ONO^{tBu})Ir(PPh_3)_2I$, 13

8 (10.5 mg, 8.24 μmol) and I_2 (2.1 mg, 8.3 μmol) were each dissolved in benzene and mixed together. The mixture was stirred at room temperature for at least 3 h, filtered, and then lyophilized. **13** (10.8 mg, 7.80 μmol, 94.6% yield) was formed as a yellow, pentane-soluble powder, although impurities can give it a green color. Crystals were obtained by allowing a pentane solution to evaporate. ^{1}H NMR (300 MHz, CD_2Cl_2): δ 0.90 (s, 18H, 2 *t*Bu on ligand phenolate), 1.15 (s, 9H, *t*Bu on ligand pyridine), 1.28 (s, 18H, 2 *t*Bu on ligand phenolate), 6.52 (d, 2H, $^4J = 2.6$ Hz, ligand phenolate aryl), 6.70 (s, 2H, ligand pyridine aryl), 6.96 (d, 2H, $^4J = 2.5$ Hz, ligand phenolate aryl), 7.08 (br s, 12H, triphenylphosphines), 7.21 (br s, 12H, triphenylphosphines), 8.16 (br s, 6H, triphenylphosphines). $^{13}C\{^1H\}$ NMR (126 MHz, CD_2Cl_2): δ 30.3, 30.4, 31.8, 34.3, 34.9, 35.7, 120.5, 124.8, 125.1, 126.6, 127.4 (br), 129.8 (br), 133.7 (br), 136.9, 137.3 (br), 141.2, 154.8, 159.2, 170.4. $^{31}P\{^1H\}$ NMR (122 MHz, C_6D_6): δ −29.1. MS FAB+: 1386.5627 (M^+), 1123.3712 ($[Ir(PPh_3)(ONO^{tBu})(I)]^+$).

2.5.1.24 Synthesis of $(ONO^{tBu})Ir(PEt_3)_2Me$, 14

12 (79.4 mg, 62.3 μmol) was dissolved in 5 mL of benzene, and PEt_3 (20 μL, 136 μmol) was added. The solution was allowed to stir for seven hours, after which the benzene and excess PEt_3 were

removed by lyophilization. The yellow powder obtained was redissolved in 5 mL of dichloromethane, and $[Rh(cod)_2]OTf$ (30.5 mg, 62.7 μmol) dissolved in 3 mL of acetonitrile was added to complex residual PEt_3. The solution was allowed to stir for three hours. Afterward, it was pumped down, and the resulting **14** was redissolved in hexanes, filtered to remove the byproducts and impurities, and pumped down again. Isolated yield was 51.4 mg (52.2 μmol, 83.7%). Crystals were obtained by allowing a pentane solution to evaporate. ^{1}H NMR (300 MHz, C_6D_6): δ 0.75 (m, 18H, 6 P$-CH_2-CH_3$), 1.16 (s, 9H, *t*Bu on ligand pyridine), 1.46 (s, 18H, 2 *t*Bu on ligand phenolate), 1.65 (m, 33H, 2 *t*Bu on ligand phenolate, 6 P$-CH_2-$CH$_3$, IrMe), 7.34 (d, 2H, $^4J = 2.6$ Hz, ligand phenolate aryl), 7.43 (s, 2H, ligand pyridine aryl), 7.53 (d, 2H, $^4J = 2.6$ Hz, ligand phenolate aryl). ^{13}C{^{1}H} NMR (126 MHz, C_6D_6): δ −33.4 (t, $J_{CP} = 8.2$ Hz), 8.1 (t, $J_{CP} = 1.5$ Hz), 13.3 (t, $J_{CP} = 14.3$ Hz), 30.6, 31.3, 32.4, 34.4, 35.3, 36.3, 118.7, 124.0, 125.6, 128.1, 136.2, 140.6, 156.3, 159.3, 172.9 (t, $J = 2.2$ Hz). ^{31}P{^{1}H} NMR (122 MHz, C_6D_6): δ −19.2. MS FAB+: 985.5609 (M^+), 867.4800 ($[Ir(PEt_3)(ONO^{tBu})(Me)]^+$). Analysis calculated for $C_{50}H_{84}IrNO_2P_2$: C, 60.95; H, 8.59; N, 1.42. Found: C, 61.18; H, 8.32; N, 1.45.

2.5.1.25 Synthesis of $(ONO^{tBu})Ir(PEt_3)_2I$, 15

14 (11.8 mg, 12.0 μmol) and **I2** (3.0 mg, 12.0 μmol) were each dissolved in benzene and mixed together. The mixture was stirred at room temperature for 5 h, filtered, and then lyophilized. **15** was formed as a yellow, pentane-soluble powder. Crystals were obtained by allowing a pentane solution to evaporate. ^{1}H NMR (300 MHz, C_6D_6): δ 0.74 (m, 18H, 6 P$-CH_2-CH_3$), 1.09 (s, 9H, *t*Bu on ligand pyridine), 1.42 (s, 18H, 2 *t*Bu on ligand phenolate), 1.71 (s, 18H, 2 *t*Bu on ligand phenolate), 1.96 (m, 12H, 6 P$-CH_2-$CH$_3$), 7.36 (s, 2H, ligand pyridine aryl), 7.37 (d, 2H, $^4J = 2.5$ Hz, ligand phenolate aryl), 7.46 (d, 2H, $^4J = 2.5$ Hz, ligand phenolate aryl). ^{13}C{^{1}H} NMR (126 MHz, C_6D_6): δ 8.4 (t, $J_{CP} = 1.6$ Hz), 15.0 (t, $J_{CP} = 15.3$ Hz), 30.0, 31.0, 31.9, 34.1, 34.9, 35.8, 118.8, 124.5, 124.7, 126.5, 137.2, 141.3, 156.3 (t, $J_{CP} = 1.4$ Hz), 159.9, 171.7 (t, $J_{CP} = 2.2$ Hz). ^{31}P{^{1}H} NMR (122 MHz, C_6D_6): δ −26.3.

The reaction of **14** and I_2 in dichloromethane gives a new species along with **15** and MeI; over the course of four days all of the **15** is converted to the new species. Crystals were obtained after the contents of the NMR tube were allowed to evaporate. X-ray crystallography, NMR, and MS support identification of this compound as the analogous chloride, $(ONO^{tBu})Ir(PEt_3)_2Cl$. ^{1}H NMR (300 MHz, CD_2Cl_2): δ 0.74 (m, 18H, 6 P$-CH_2-CH_3$), 1.01 (m, 12H, 6 P$-CH_2-$CH$_3$), 1.33 (s, 18H, 2 *t*Bu on ligand phenolate), 1.37 (s, 18H, 2 *t*Bu on ligand phenolate), 1.38 (s, 9H, *t*Bu on ligand pyridine), 7.11 (d, 2H, $^4J = 2.5$ Hz, ligand phenolate aryl), 7.26 (d, 2H, $^4J = 2.5$ Hz, ligand phenolate aryl), 7.31 (s, 2H, ligand pyridine aryl). ^{13}C{^{1}H} NMR (126 MHz, CD_2Cl_2): δ 7.7, 13.0 (t, $J_{CP} = 15.1$ Hz), 30.5, 30.6, 31.9, 34.4, 35.5, 35.9, 119.4, 124.6, 124.8, 126.6, 137.6, 140.3, 157.0, 160.5, 171.7. ^{31}P{^{1}H} NMR (122 MHz, CD_2Cl_2): δ −20.7. MS FAB+ 970.5417 ($[Ir(PEt_3)_2(ONO^{tBu})]^+$), 887.3802 ($[Ir(PEt_3)(ONO^{tBu})(Cl)]^+$), 852.4370 ($[Ir(PEt_3)(ONO^{tBu})]^+$).

2.5.1.26 Synthesis of $[(ONO^{tBu})Ir(PEt_3)_2Me]PF_6$, 16

14 (31.8 mg, 32.3 μmol) was dissolved in dichloromethane, and a dichloromethane suspension of $AgPF_6$ (8.1 mg, 32 μmol) was added. The mixture was allowed to stir for one hour before being pumped down. It was then redissolved in a small amount of benzene and filtered. The solution was then layered with pentane and allowed to sit overnight. Dark blue needle-like crystals of **16**·2 C_6H_6 (39.1 mg, 30.4 μmol, 94.1% yield) were recovered. ^{1}H NMR (300 MHz, CD_2Cl_2): δ −3.1 (very broad), −2.0 (broad), 0.73, 3.99, 12.0 (very broad). $^{19}F\{^{13}C\}$ NMR (282 MHz, CD_2Cl_2): δ −73.8 (d, $^1J_{PF}$ = 710 Hz). $^{31}P\{^1H\}$ NMR (122 MHz, CD_2Cl_2): δ −144.7 (septet, $^1J_{PF}$ = 710 Hz). MS FAB+: 985.5561 (M^+), 867.4697 ($[Ir(PEt_3)(ONO^{tBu})(Me)]^+$).

2.5.1.27 Synthesis of $(ONO^{tBu})Ir(PPh_3)_2Ph$, 17

12 (20.4 mg, 16.0 μmol) was dissolved in 10 mL of benzene and stirred in a 65°C oil bath for 24 h. The solution was reintroduced into the glovebox, and the solvent was removed. The residue was redissolved in pentane and filtered, and the solution pumped down to obtain **17** (20.9 mg, 15.6 μmol, 98% yield). Crystals were obtained by allowing a pentane solution to evaporate. ^{1}H NMR (300 MHz, CD_2Cl_2): δ 0.70 (s, 18H, 2 *t*Bu on ligand phenolate), 1.20 (s, 9H, *t*Bu on ligand pyridine), 1.43 (s, 18H, 2 *t*Bu on ligand phenolate), 5.83 (br s, 2H, IrPh), 6.54 (br s, 1H, IrPh), 6.62 (d, 2H, ^4J = 2.7 Hz, ligand phenolate aryl), 6.78 (s, 2H, ligand pyridine aryl), 6.8 − 7.1 (multiple broad peaks, 30H, triphenylphosphines), 7.16 (d, 2H, ^4J = 2.6 Hz, ligand phenolate aryl), 7.29 (br s, 2H, IrPh). $^{13}C\{^1H\}$ NMR (126 MHz, C_6D_6): δ 30.3, 30.6, 32.2, 34.2, 34.4, 35.9, 120.4, 123.6, 124.1, 125.6, 125.9, 126.9, 127.0, 129.6, 129.7, 133.3 (br), 135.7, 136.5 (br), 141.2, 145.9, 155.3, 157.7, 171.5. $^{31}P\{^1H\}$ NMR (122 MHz, CD_2Cl_2): δ −13.2.

2.5.1.28 Reaction of 12 with Toluene

12 (7.8 mg, 6.1 μmol) was dissolved in 700 μL of toluene-d_8 in a J-Young NMR tube. The tube was heated at 65°C and periodically monitored by ^{1}H NMR until all starting material signals had disappeared, which took six days; the final ^{1}H NMR spectrum was complex. The mass spectrum of the solid obtained by evaporation exhibited a signal indicating the presence of the analogous tolyl complex (1094.5436, $[Ir(PPh_3)(ONO^{tBu})(C_6D_4CD_3]^+$, $[M-PPh_3]^+$), while the $^{31}P\{^1H\}$ NMR of the dissolved solid showed two approximately equal signals at δ −12.2 and −12.3, tentatively assigned to meta and para isomers. A much weaker signal at −12.8 may indicate formation of a very small amount of ortho isomer. Isolation of a pure product was not achieved.

2.5.1.29 Synthesis of $(ONO^{tBu})Ir(PPh_3)[\kappa^2\text{-}(o\text{-}C_6H_4)PPh_2]$, 18

12 (8.2 mg, 6.4 μmol) was dissolved in 1 mL of CD_2Cl_2 in a J-Young NMR tube and submerged in a 65°C oil bath for 21 h. After NMR confirmation that the reaction was complete, the solvent was removed to obtain **18** (7.7 mg, 6.1 μmol, 95% isolated yield). Crystals were obtained by allowing a pentane solution to evaporate. ^{1}H NMR (500 MHz, CD_2Cl_2): δ 0.47 (s, 18H, 2 tBu on ligand phenolate), 1.27 (s, 18H, 2 tBu on ligand phenolate), 1.34 (s, 9H, tBu on ligand pyridine), 6.64 (m, 4H, triphenylphosphines), $6.9-7.4$ (many multiplets, 23H, triphenylphosphines), 7.50 (dd, $^3J = 4.4$ Hz, $^3J = 6.6$ Hz, 2H, triphenylphosphines). $^{13}C\{^1H\}$ NMR (126 MHz, CD_2Cl_2): δ 29.58, 30.76, 32.11, 34.24, 35.27, 35.32, 119.51, 119.69, 122.48, 122.55, 123.83, 124.00, 125.60, 125.77, 128.32, 128.39, 129.03, 129.54, 133.76, 133.83, 136.03, 139.93, 140.51, 140.61, 152.80, 153.23, 154.77, 159.36, 170.44. $^{31}P\{^1H\}$ NMR (122 MHz, CD_2Cl_2): δ −69.5 (d, $^2J_{PP} = 448$ Hz), −2.5 (d, $^2J_{PP} = 448$ Hz). MS FAB+: 1257.5292 (M^+), 995.4405 ($[Ir(PPh_3)(ONO^{tBu})]^+$).

2.5.1.30 Synthesis of $[(ONO^{tBu})Ir(PPh_3)(CH_2CN)]_2$, 19

12 (13.1 mg, 10.3 μmol) was dissolved in 1 mL of CD_2Cl_2 in a J-Young NMR tube, and 40 μL of acetonitrile was added. The tube was then submerged in a 65°C oil bath for 72 h. After NMR confirmation that the reaction had completed, $[Rh(cod)_2]OTf$ (2.6 mg, 5.3 μmol) dissolved in 1 mL of acetonitrile was added. The solution was allowed to stir for three hours. Afterward, it was pumped down, and the resulting **19** was redissolved in hexanes, filtered to remove the byproducts and impurities, and pumped down again. Crystals were obtained by allowing a pentane solution to evaporate. Isolated yield was 91% (9.7 mg, 4.7 μmol). ^{1}H NMR (500 MHz, CD_2Cl_2): δ 1.23 (s, 9H, 2 tBu on ligand), 1.25 (s, 9H, 2 tBu on ligand), 1.43 (s, 9H, 2 tBu on ligand), 1.44 (s, 9H, 2 tBu on ligand), 1.55 (s, 9H, 2 tBu on ligand), 1.87 (s, 2H, Ir−CH_2−CN), 6.4-6.5 (m, 3H, triphenylphosphine), 6.7-6.8 (m, 3H, triphenylphosphine), 6.9-7.1 (m, 6H, triphenylphosphine),7.2-7.5 (m, 6H, triphenylphosphine), 7.6-7.8 (m, 2H, triphenylphosphine), 7.9-8.1 (m, ^{1}H, triphenylphosphine). $^{13}C\{^1H\}$ NMR (126 MHz, CD_2Cl_2): δ 3.4, 30.1, 30.3, 30.5, 31.9, 32.2, 34.2, 34.6, 35.2, 35.7, 35.9, 116.0, 118.0, 120.2, 122.5, 123.5, 125.6, 126.0, $128-130$ (br), 135.0, 138.0, 138.7, 141.1 (d, $J_{CP} = 3.8$ Hz), 153.9, 154.4, 158.2, 159.8 (d, $J_{CP} = 2.7$ Hz), 161.1, 167.6 (d, $J_{CP} = 3.4$ Hz), 170.8 (d, $J_{CP} = 1.0$ Hz). $^{31}P\{^1H\}$ NMR (122 MHz, CD_2Cl_2): δ −88.3.

2.5.1.31 Kinetic Experiments

Kinetic experiments were carried out with 8.8 mM solutions of **12** or **14**. In a typical example, 7.8 mg (6.1 μmol) **12** was dissolved in 700 μL of C_6D_6 inside a nitrogen-filled glovebox, and the solution was transferred to a J-Young NMR tube. The NMR tube was then removed from the glovebox and fully submerged in a 65°C ethylene glycol bath. The reactions were periodically halted by transferring the

Entry[a]	eq PPh_3[b]	$[PPh_3]$[c]	k^d_{obs}	R^2
a	0.000	0	2.18×10^{-4}	0.9937
b	0.125	1.1	1.54×10^{-5}	0.9965
c	0.250	2.2	1.19×10^{-5}	0.9842
d	0.375	3.3	6.27×10^{-6}	0.9964
e	0.500	4.4	5.28×10^{-6}	0.9910
f	0.500	4.4	5.77×10^{-6}	0.9921
g	0.625	5.4	4.14×10^{-6}	0.9877
h	0.750	6.5	2.58×10^{-6}	0.9768
i	0.750	6.5	3.14×10^{-6}	0.9912
j	0.875	7.6	2.32×10^{-6}	0.9904
k	1.000	8.7	1.88×10^{-6}	0.9821
l	1.125	9.8	1.90×10^{-6}	0.9558
m	1.250	10.9	1.70×10^{-6}	0.9777

Table 2.1. Summary of the results of Figure 2.23, used to create Figure 2.21. a) The particular run is detailed in the corresponding section in Figure 2.23; b) equivalents of PPh_3 added; c) concentration of added PPh_3 in mM. d) the k_{obs} value, in s^{-1}, calculated by fitting the curve to the first-order rate equation $[\mathbf{12}] = [\mathbf{12}]_0 \exp(-k_{obs}t)$.

NMR tube into an ice bath before NMR measurements. The progress of the reactions were measured by ^{31}P NMR integration, with NOE turned off and the d1 time set to 22.895 s (**12** has the longest relaxation time, 4.579 s, of all the relevant iridium compounds). For PPh_3 inhibition experiments, the Ir complex was mixed with various amounts of a 20 mg/mL stock solution of PPh_3 in C_6D_6, and additional C_6D_6 was added to bring the volume up to 700 μL.

2.5.2 Kinetics Details

Figure 2.21 was constructed from the data in table 2.1. The entries in this table were obtained from individual runs detailed in Figure 2.23.

2.5.3 Crystallographic Data

Crystallographic data for the complexes **4**, **5**, **6**, **7**, **8**, **9**, **10**, **11**, **12**, **13**, **14**, **15**, **16**, **17**, **18**, **19**, and $(ONO^{tBu})Ir(PEt_3)_2Cl$ are found in the following tables 2.2, 2.3, 2.4, 2.5, and 2.6.

2.6 Acknowledgments

We thank Dr. Michael W. Day and Lawrence M. Henling (Caltech) for X-ray crystallographic studies. The Bruker KAPPA APEXII X-ray diffractometer was purchased *via* an NSF CRIF:MU award to the California Institute of Technology, CHE-0639094. This work was supported by BP in the MC_2 and XC_2 programs.

Figure 2.23. Conversion of **12** to **17**-d_6 in C_6D_6 with varying amounts of extra PPh_3 added. $[\mathbf{12}]_0 = 8.7$ mM. a) $[PPh_3]_0 = 0$ mM, b) $[PPh_3]_0 = 1.1$ mM, c) $[PPh_3]_0 = 2.2$ mM, d) $[PPh_3]_0 = 3.3$ mM, e) $[PPh_3]_0 = 4.4$ mM, f) $[PPh_3]_0 = 4.4$ mM, g) $[PPh_3]_0 = 5.4$ mM, h) $[PPh_3]_0 = 6.5$ mM, i) $[PPh_3]_0 = 6.5$ mM, j) $[PPh_3]_0 = 7.6$ mM, k) $[PPh_3]_0 = 8.7$ mM, l) $[PPh_3]_0 = 9.8$ mM, m) $[PPh_3]_0 = 10.9$ mM.

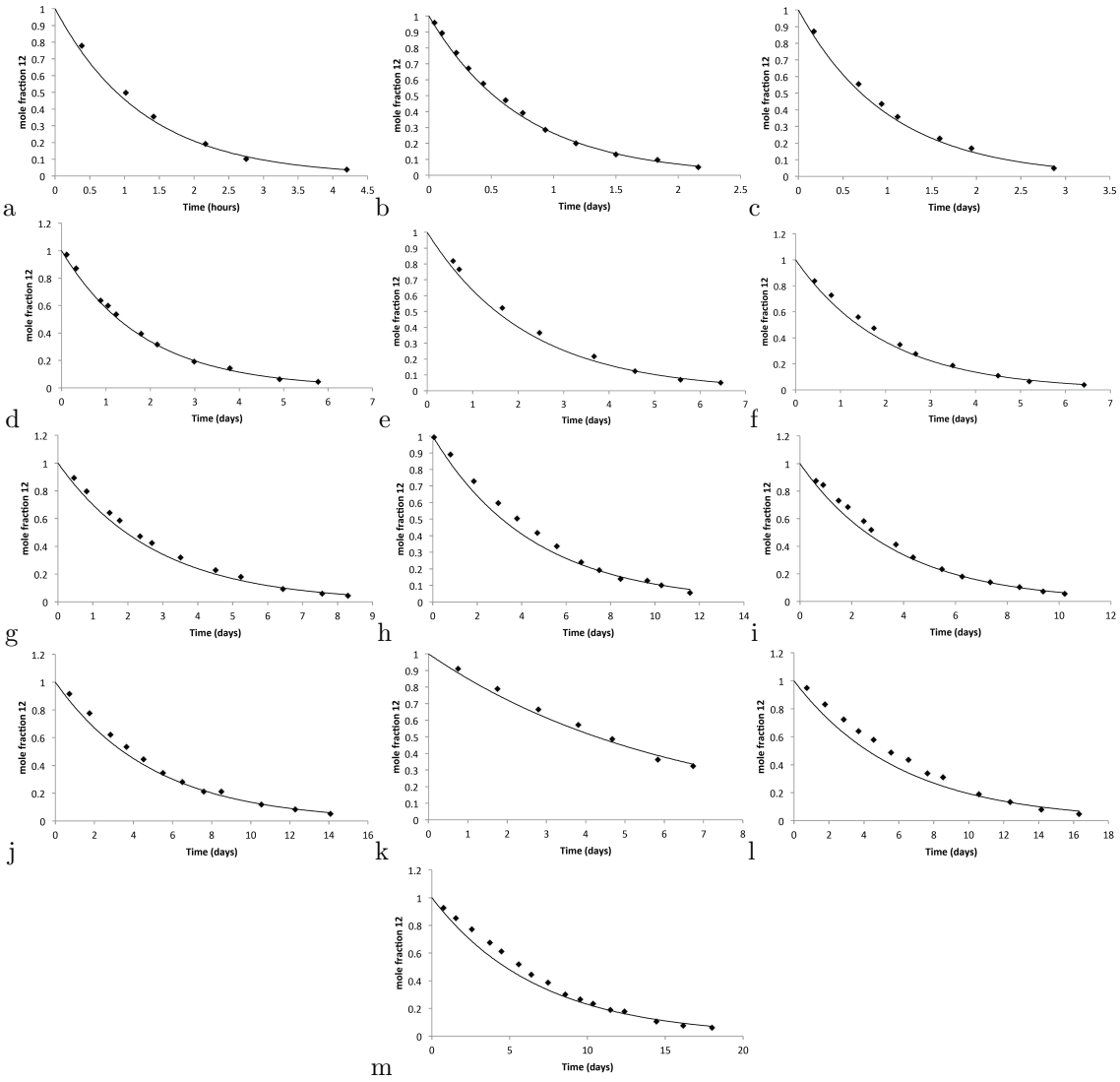

	4	**5**	**6**	**7**
Empirical formula	$C_{90}H_{126}N_2O_4Ir_2 \cdot 2\,Na \cdot C_4H_{10}O$	$C_{53}H_{75}NO_2Ir_2$	$[C_{47}H_{66}N_2O_2Ir][PF_6] \cdot C_6H_6$	$C_{46}H_{63}F_3NO_5SIr \cdot 1.5(C_6H_6)$
Formula weight	1804.43	1142.54	1106.30	1108.40
Crystal structure	Monoclinic	Monoclinic	Triclinic	Triclinic
Lattice parameters				
a (Å)	29.8716(11)	9.5497(4)	11.0592(5)	11.7099(4)
b (Å)	14.4205(5)	22.3182(9)	11.8291(5)	13.1880(5)
c (Å)	24.4163(15)	22.9384(10)	20.4215(9)	17.2153(6)
α (°)	90	90	105.154(2)	86.059(2)
β (°)	123.7310(10)	92.086(2)	97.156(2)	72.263(2)
γ (°)	90	90	95.370(2)	87.034(2)
Volume (Å^3)	8747.0(7)	4885.7(4)	2536.27(19)	2524.87(16)
Space group	$C2/c$	$P2_1/n$	$P1$	$P1$
Z value	4	4	2	2
ρ_{calc} (g/cm^3)	1.370	1.553	1.449	1.458
μ (mm^{-1})	3.100	5.481	2.727	2.744
Temperature (K)	100(2)	100(2)	100(2)	100(2)
θ range (°)	1.66 to 35.19	1.82 to 35.82	1.80 to 40.84	1.55 to 43.59
No. obs. ($I > 2\sigma(I)$)	15255	19264	26070	34153
No. parameters	485	533	874	883
Goodness of fit*	3.747	1.885	1.957	1.536
Max. shift in cycle	0.003	0.007	0.016	0.015
Residuals*: R, R_w	0.0314; 0.0719	0.0355; 0.0535	0.0206; 0.0392	0.0221; 0.0381
Absorption correction	Semi-empirical from equivalents	Semi-empirical from equivalents	Semi-empirical from equivalents	Semi-empirical from equivalents
max/min	0.7469; 0.5672	0.7470; 0.5076	0.7480; 0.5945	0.7486; 0.6139
Largest peak & hole (e$^-$/Å^3)	2.370; −1.617	2.894; −2.135	2.557; −1.524	2.541; −1.556

Table 2.2. * $R = \frac{\sum_{hkl}||F_{obs}|-|F_{calc}||}{\sum_{hkl}|F_{obs}|}$; $R_w = \sqrt{\frac{\sum_{hkl} w(|F_{obs}|-|F_{calc}|)^2}{\sum_{hkl} wF_{obs}^2}}$, $w = 1/\sigma^2(F_{obs})$; GOF $= \sqrt{\frac{\sum_{hkl} w(|F_{obs}|-|F_{calc}|)^2}{n_{data}-n_{vari}}}$.

	8	**9**	**10**	**11**
Empirical formula	$C_{74}H_{81}F_3NO_5P_2SIr \cdot 0.53(C_5H_{12}) \cdot 1.47(C_6H_6)$	$C_{73}H_{82}NO_3P_2Ir$	$C_{73}H_{81}NO_2P_2ClIr \cdot 5\,(CH_2Cl_2)$	$C_{73}H_{82}NO_2P_2Ir \cdot C_5H_{12}$
Formula weight	1560.64	1275.54	1718.61	1331.68
Crystal structure	Monoclinic	Monoclinic	Monoclinic	Monoclinic
Lattice parameters				
a (Å)	12.9942(5)	13.0223(4)	19.3956(9)	16.8289(8)
b (Å)	22.9825(9)	21.0636(7)	13.1877(6)	23.8694(10)
c (Å)	25.8969(9)	22.7792(8)	31.5557(15)	17.4749(8)
α (°)	90	90	90	90
β (°)	103.513(2)	99.1960(10)	106.611(2)	102.373(2)
γ (°)	90	90	90	90
Volume (Å^3)	7519.7(5)	6167.9(4)	7734.6(6)	6856.5(5)
Space group	$P2_1/n$	$P2_1/n$	$P2_1/c$	$P2_1/n$
Z value	4	4	4	4
ρ_{calc} (g/cm^3)	1.379	1.374	1.476	1.290
μ (mm^{-1})	1.906	2.265	2.194	2.040
Temperature (K)	100(2)	100(2)	100(2)	100(2)
θ range (°)	1.84 to 31.76	2.41 to 29.67	1.35 to 37.99	1.47 to 33.55
No. obs. ($I > 2\sigma(I)$)	18398	14018	32658	19762
No. parameters	966	1049	871	1086
Goodness of fit*	2.750	1.713	2.152	2.140
Max. shift in cycle	0.002	0.004	0.011	0.004
Residuals*: R, R_w	0.0463; 0.0958	0.0238; 0.0373	0.0340; 0.0589	0.0310; 0.0519
Absorption correction	Semi-empirical from equivalents	Semi-empirical from equivalents	Semi-empirical from equivalents	Semi-empirical from equivalents
max/min	0.7463; 0.6010	0.7459; 0.6381	0.7474; 0.6430	0.7466; 0.6219
Largest peak & hole (e$^-$/Å^3)	3.915; −2.838	2.894; −0.696	3.136; −2.303	2.907; −2.314

Table 2.3. * $R = \frac{\sum_{hkl}||F_{\text{obs}}|-|F_{\text{calc}}||}{\sum_{hkl}|F_{\text{obs}}|}$; $R_w = \sqrt{\frac{\sum_{hkl} w(|F_{\text{obs}}|-|F_{\text{calc}}|)^2}{\sum_{hkl} wF_{\text{obs}}^2}}$, $w = 1/\sigma^2(F_{\text{obs}})$; GOF $= \sqrt{\frac{\sum_{hkl} w(|F_{\text{obs}}|-|F_{\text{calc}}|)^2}{n_{\text{data}}-n_{\text{vari}}}}$.

	12	**13**	**14**	**15**
Empirical formula	$C_{74}H_{84}NO_2P_2Ir$	$C_{73}H_{81}INO_2P_2Ir \cdot 2\,(C_5H_{12})$	$C_{50}H_{84}NO_2P_2Ir$	$0.67(C_{49}H_{80}INO_2P_2Ir)$; $0.33(C_{50}H_{83}NO_2P_2Ir)$
Formula weight	1273.56	1529.72	985.32	1097.19
Crystal structure	Monoclinic	Monoclinic	Monoclinic	Monoclinic
Lattice parameters				
a (Å)	13.1981(7)	14.4250(5)	12.2897(7)	12.2460(6)
b (Å)	20.9991(9)	19.4180(6)	35.3664(19)	35.7358(18)
c (Å)	22.8801(12)	26.3735(9)	11.4244(6)	11.4544(6)
α (°)	90	90	90	90
β (°)	100.388(3)	99.362(2)	93.830(2)	93.490(2)
γ (°)	90	90	90	90
Volume (Å^3)	6237.2(5)	7288.9(4)	4954.4(5)	6856.5(5)
Space group	$P2_1/n$	$P2_1/c$	$P2_1/c$	$P2_1/c$
Z value	4	4	4	4
ρ_{calc} (g/cm^3)	1.356	1.394	1.321	1.457
μ (mm^{-1})	2.239	2.346	2.796	3.386
Temperature (K)	100(2)	100(2)	100(2)	100(2)
θ range (°)	1.66 to 29.33	1.57 to 28.67	1.76 to 27.89	1.87 to 40.01
No. obs. ($I > 2\sigma(I)$)	10617	15318	10841	25951
No. parameters	737	848	527	537
Goodness of fit*	1.268	2.742	1.824	1.448
Max. shift in cycle	0.003	0.002	0.003	0.010
Residuals*: R, R_w	0.0387; 0.0478	0.0482; 0.0750	0.0188; 0.0366	0.0344; 0.0620
Absorption correction	Semi-empirical from equivalents	Semi-empirical from equivalents	Semi-empirical from equivalents	Semi-empirical from equivalents
max/min	0.7459; 0.6362	0.4314; 0.3230	0.7456; 0.6727	0.7479; 0.6295
Largest peak & hole (e$^-$/Å^3)	1.724; −1.487	1.880; −2.150	0.633; −0.778	2.448; −2.844

Table 2.4. * $R = \frac{\sum_{hkl}||F_{\mathrm{obs}}|-|F_{\mathrm{calc}}||}{\sum_{hkl}|F_{\mathrm{obs}}|}$; $R_w = \sqrt{\frac{\sum_{hkl} w(|F_{\mathrm{obs}}|-|F_{\mathrm{calc}}|)^2}{\sum_{hkl} wF_{\mathrm{obs}}^2}}$, $w = 1/\sigma^2(F_{\mathrm{obs}})$; GOF $= \sqrt{\frac{\sum_{hkl} w(|F_{\mathrm{obs}}|-|F_{\mathrm{calc}}|)^2}{n_{\mathrm{data}}-n_{\mathrm{vari}}}}$.

	16	**17**	**18**	**19**
Empirical formula	$[C_{50}H_{84}NO_2P_2Ir][PF_6] \cdot 1.5(C_6H_6)$	$C_{79}H_{86}NO_2P_2Ir \cdot 2\,(C_6H_6)$	$C_{73}H_{80}NO_2P_2Ir$	$C_{114}H_{136}Li_2N_4O_4P_2Ir_2$
Formula weight	1249.08	745.92	1257.52	2086.49
Crystal structure	Triclinic	Orthorhombic	Monoclinic	Triclinic
Lattice parameters				
a (Å)	21.3366(12)	16.0771(8)	41.3489(19)	16.4557(8)
b (Å)	21.4842(13)	20.5290(10	18.8871(9)	17.2824(8)
c (Å)	26.6266(15)	23.1672(11)	20.6067(9)	21.7560(10)
α (°)	81.836(4)	90	90	93.951(2)
β (°)	85.844(3)	90	111.731(2)	96.184(3)
γ (°)	89.459(4)	90	90	101.190(3)
Volume (Å^3)	12050.2(12)	7646.3(6)	14949.3(12)	6008.7(5)
Space group	$P1$	$Pbcn$	$C2/c$	$P1$
Z value	8	8	8	2
ρ_{calc} (g/cm^3)	1.377	1.296	1.117	1.153
μ (mm^{-1})	2.354	1.837	1.867	2.284
Temperature (K)	100(2)	100(2)	100(2)	100(2)
θ range (°)	1.66 to 27.99	1.76 to 37.38	1.47 to 32.01	2.34 to 34.09
No. obs. ($I > 2\sigma(I)$)	37498	13314	20406	30107
No. parameters	2386	417	758	1176
Goodness of fit*	1.780	3.326	2.133	2.866
Max. shift in cycle	0.003	0.001	0.008	0.007
Residuals*: R, R_w	0.0739; 0.1072	0.0443; 0.0804	0.0311; 0.0569	0.0335; 0.0589
Absorption correction	Semi-empirical from equivalents	Semi-empirical from equivalents	Semi-empirical from equivalents	Semi-empirical from equivalents
max/min	0.8340; 0.6254	0.7473; 0.6479	0.7463; 0.6478	0.7461; 0.6684
Largest peak & hole (e$^-$/Å^3)	2.889; −2.188	4.097; −2.794	1.457; −0.873	1.933; −1.882

Table 2.5. * $R = \frac{\sum_{hkl}||F_{\text{obs}}|-|F_{\text{calc}}||}{\sum_{hkl}|F_{\text{obs}}|}$; $R_w = \sqrt{\frac{\sum_{hkl} w(|F_{\text{obs}}|-|F_{\text{calc}}|)^2}{\sum_{hkl} wF_{\text{obs}}^2}}$, $w = 1/\sigma^2(F_{\text{obs}})$; GOF $= \sqrt{\frac{\sum_{hkl} w(|F_{\text{obs}}|-|F_{\text{calc}}|)^2}{n_{\text{data}}-n_{\text{vari}}}}$.

	$(ONO^{tBu})Ir(PEt_3)_2Cl$
Empirical formula	$C_{49}H_{81}ClNO_2P_2Ir$
Formula weight	1005.74
Crystal structure	Monoclinic
Lattice parameters	
a (Å)	12.2623(6)
b (Å)	35.4340(17)
c (Å)	11.3773(6)
α (°)	90
β (°)	93.368(2)
γ (°)	90
Volume (Å^3)	4934.9(4)
Space group	$P2_1/c$
Z value	4
ρ_{calc} (g/cm^3)	1.354
μ (mm^{-1})	2.861
Temperature (K)	100(2)
θ range (°)	1.88 to 39.87
No. obs. ($I > 2\sigma(I)$)	26158
No. parameters	526
Goodness of fit*	2.079
Max. shift in cycle	0.003
Residuals*: R, R_w	0.0371; 0.0602
Absorption correction	Semi-empirical from equivalents
max/min	0.7478; 0.5515
Largest peak & hole (e$^-$/Å^3)	2.623; −2.981

Table 2.6. * $R = \frac{\sum_{hkl}||F_{obs}|-|F_{calc}||}{\sum_{hkl}|F_{obs}|}$; $R_w = \sqrt{\frac{\sum_{hkl} w(|F_{obs}|-|F_{calc}|)^2}{\sum_{hkl} wF_{obs}^2}}$, $w = 1/\sigma^2(F_{obs})$; GOF $= \sqrt{\frac{\sum_{hkl} w(|F_{obs}|-|F_{calc}|)^2}{n_{data}-n_{vari}}}$.

2.7 References

[1] (a) Labinger, J. A.; Bercaw, J. E. *Nature* **2002**, *417*, 507–514;

(b) Crabtree, R. H. *J. Chem. Soc., Dalton Trans.* **2001**, 2437–2450;

(c) Labinger, J. A. *Fuel Proc. Technol. 1995*, *42*, 325–338;

(d) Labinger, J. A. *J. Mol. Catal.* **2004**, *220*, 27–35.

[2] (a) Fekl, U.; Goldberg, K. I. *Adv. Inorg. Chem.* **2003**, *54*, 259–320;

(b) Lersch, M.; Tilset, M. *Chem. Rev.* **2005**, *105*, 2471–2526.

[3] (a) Goldshlegger, N. F.; Tyabin, M. B.; Shilov, A. E.; Shteinman, A. A. *Zh. Fiz. Khim.* **1969**, *43*, 2174–2175;

(b) Goldshlegger, N. F.; Eskova, V. V.; Shilov, A. E.; Shteinman, A. A. *Zh. Fiz. Khim.* **1972**, *46*, 1353–1354;

(c) Shilov, A. E.; Shul'pin, G. B. *Activation and Catalytic Reactions of Saturated Hydrocarbons in the Presence of Metal Complexes*; Kluwer Academic Publishers: Dordrecht, **2000**; pp. 259–317.

[4] Periana, R. A.; Taube, D. J.; Evitt, E. R.; Loffler, D. G.; Wentrcek, P. R.; Voss, G.; Masuda, T. *Science* **1993**, *259*, 340–343.

[5] Arndtsen, B. A.; Bergman, R. G.; Mobley, T. A.; Peterson, T. H. *Acc. Chem. Res.* **1995**, *28*, 154–162.

[6] (a) Wong-Foy, A. G.; Bhalla, G.; Liu, X. Y.; Periana, R. A. *J. Am. Chem. Soc.* **2003**, *125*, 14292–14293;

(b) Oxgaard, J.; Muller, R. P.; Goddard, W. A.; Periana, R. A. *J. Am. Chem. Soc.* **2004**, *126*, 352–363;

(c) Bhalla, G.; Liu, X. Y.; Oxgaard, J.; Goddard, W. A.; Periana, R. A. *J. Am. Chem. Soc.* **2005**, *127*, 11372–11389;

(d) Tenn, W. J.; Young, K. J. H.; Bhalla, G.; Oxgaard, J.; Goddard, W. A.; Periana, R. A. *J. Am. Chem. Soc.* **2005**, *127*, 14172–14173;

(e) Bhalla, G.; Periana, R. A. *Angew. Chem., Int. Ed.* **2005**, *44*, 1540–1543;

(f) Young, K. J. H.; Mironov, O. A; Periana, R. A. *Organometallics* **2007**, *26*, 2137–2140;

(g) Young, K. J. H.; Oxgaard, J.; Ess, D. H.; Meier, S. K.; Stewart, T.; Goddard, W. A.; Periana, R. A. *Chem. Commun.* **2009**, 3270–3272.

[7] (a) Agapie, T.; Day, M. W.; Bercaw, J. E. *Organometallics* **2008**, *27*, 6123–6142;

(b) Agapie, T.; Henling, L. H.; DiPasquale, A. G.; Rheingold, A. L.; Bercaw, J. E. *Organometallics* **2008**, *27*, 6245–6256.

[8] Weinberg, D. R.; Hazari, N.; Labinger, J. A.; Bercaw, J. E. *Organometallics* **2010**, *29*, 89–100.

[9] The synthesis of H_2(ONO) was first reported in: Agapie, T. Ph.D. Thesis, California Institute of Technology, Pasadena, CA, **2007**, pp. 156–159, 214–215.

[10] Danopoulos, A. A.; Winston, S.; Hursthouse, M. B. *J. Chem. Soc., Dalton Trans.* **2002**, 3090–3091.

[11] Hughes, R. P.; Kovacik, I.; Lindner, D. C.; Smith, J. M.; Willemsen, S.; Zhang, D.; Guzei, I. A.; Rheingold, A. L. *Organometallics* **2001**, *20*, 3190–3197.

[12] Recent calculations have indicated that β-hydride elimination from some methoxide complexes may be energetically disfavored: Theophanis, P. L.; Goddard, W. A. *Organometallics* **2011**, *30*, 4941–4948, although there are many examples in the literature.

[13] Lu, Z; Jun, C-H; de Gala, S. R.; Sigalas, M. P.; Eisenstein, O; Crabtree, R. H. *Organometallics* **1995**, *14*, 1168–1175.

[14] The crystal structure included a complex solvent region that could not be satisfactorily modeled and also showed the presence of Li^+ ions, presumably carried along as impurities from an earlier step in the overall synthetic sequence; the required charge-balancing counteranions could not be located, probably because they lie within the solvent region. However, determination of the molecular structure of the Ir_2 complex **19** was unproblematic.

[15] A somewhat related situation has been described previously: Luecke, H. F.; Bergman, R. G. *J. Am. Chem. Soc.* **1997**, *119*, 11538–11539. The cyclometalated Ir^{III} complex Cp*(OTf)Ir(κ^2-PPh_2(*o*-C_6H_4)), obtained from the room-temperature reaction of

Cp*(OTf)Ir(PPh_3)Me in CH_2Cl_2, reacts with benzene to form Cp*(OTf)Ir(PPh_3)Ph. Here however the intermolecular activation product is thermodynamically preferred; probably the difference between the two systems is primarily of steric origin, as both include ligands (*tert*-butyl substituents on ONO; the large Cp* group) that can lead to severe crowding.

[16] Golden, J. T.; Andersen, R. A.; Bergman, R. G. *J. Am. Chem. Soc.* **2001**, *123*, 5837–5838.

[17] (a) Stour, D. L.; Zaric, S.; Niu, S. Q.; Hall, M. B. *J. Am. Chem. Soc.* **1996**, *118*, 6068–6069; (b) Su, M. D.; Chu, S. Y. *J. Am. Chem. Soc.* **1997**, *119*, 5373–5383.

[18] Pangborn, A. B.; Giardello, M. A.; Grubbs, R. H.; Rosen, R. K.; Timmers, F. J. *Organometallics* **1996**, *15*, 1518–1520.

[19] Ko, P.-H.; Chen, T.-Y.; Zhu, J.; Cheng, K.-F.; Peng, S.-M.; Che, C.-M. *J. Chem. Soc., Dalton Trans.* **1995**, 2215–2220.